INVITED PAPER

Wireless Myths, Realities, and Futures: From 3G/4G to Optical and Quantum Wireless

This paper evaluates both the operational third-generation (3G) as well as the emerging fourth-generation (4G) wireless systems and investigates new technologies that might transpire and change things in the future.

By Lajos Hanzo, *Fellow IEEE*, Harald Haas, *Member IEEE*, Sándor Imre, *Member IEEE*, Dominic O'Brien, *Member IEEE*, Markus Rupp, *Senior Member IEEE*, and Laszlo Gyongyosi, *Member IEEE*

"*It is difficult to make predictions, especially about the future.*"—*Mark Twain*

ABSTRACT |

1) *The Myth*: Sixty years of research following Shannon's pioneering paper has led to telecommunications solutions operating arbitrarily close to the channel capacity—"flawless telepresence" with *zero error* is available to anyone, anywhere, anytime across the globe.
2) *The Reality*: Once we leave home or the office, even top of the range iPhones and tablet computers fail to maintain "flawless telepresence" quality. They also fail to approach the theoretical performance predictions. The 1000-fold throughput increase of the best third-generation (3G) phones over second-generation (2G) GSM phones and the 1000-fold increased teletraffic predictions of the next decade require substantial further bandwidth expansion toward ever increasing carrier frequencies, expanding beyond the radio-frequency (RF) band to optical frequencies, where substantial bandwidths are available.
3) *The Future*: However, optical- and quantum-domain wireless communications is less developed than RF wireless. It is also widely recognized that the pathloss of RF wireless systems monotonically increases with the carrier frequency and this additional challenge has to be tackled by appropriate countermeasures in future research. Hence, we set out to seek promising techniques of tackling the aforementioned challenges and for resolving the conflicting design constraints imposed on the flawless telepresence systems of the future. *To disspell the myth*, we evaluate both the operational 3G as well as the emerging fourth-generation (4G) wireless systems and demonstrate that there is a substantial difference between their theoretical and their practically attainable performance. *The reality is* that the teletraffic predictions indicate further thirst for bandwidth, which cannot be readily satisfied within the most popular 1–2-GHz carrier-frequency range, where the best propagation conditions prevail. We briefly consider the 10–300-GHz unlicensed band as a potential source of further spectrum, followed by a review of advances way beyond the upper edge of the RF range at 300 GHz, namely to the realms of optical wireless (OW) communications. As the carrier frequency is increased, the pathloss is also increased, which results in ever smaller cells.

Manuscript received January 26, 2012; accepted February 7, 2012. Date of publication April 27, 2012; date of current version May 10, 2012.
L. Hanzo is with the School of Electronics and Computer Science, University of Southampton, Southampton SO17 1BJ, U.K. (e-mail: lh@ecs.soton.ac.uk).
H. Haas is with The University of Edinburgh, Edinburgh EH9 3JL, U.K. (e-mail: h.haas@ed.ac.uk).
S. Imre is with the Telecommunications Department, Budapest University of Technology and Economics, Budapest 1521, Hungary.
D. O'Brien is with the Department of Engineering Science, University of Oxford, Oxford OX1 3PJ, U.K. (e-mail: dominic.obrien@eng.ox.ac.uk).
M. Rupp is with the Institute of Telecommunications, Technische Universität Wien, Wien A-1040, Austria (e-mail: markus.rupp@tuwien.ac.at).
L. Gyongyosi is with the Faculty of Electrical Engineering and Informatics, Department of Telecommunications, Budapest University of Technology and Economics, Budapest 1521, Hungary (e-mail: gyongyosi@hit.bme.hu).
Digital Object Identifier: 10.1109/JPROC.2012.2189788

Furthermore, the high-frequency RF waves predominantly obey line-of-sight (LOS) propagation—like visible light. *The future* requires advances in both infrared and visible-light communications for circumventing the LOS nature of light. We hypothesize that light-emitting diode (LED) arrays acting as "massive" multiple-input–multiple-output (MIMO) components as well as transmitter/receiver cooperation might be conceived. The heterogeneous networks of the near future will rely on seamless, near-instantaneous handovers among OW hotspots, RF hotspots, and oversailing larger cells. These "massive" MIMOs might impose a high complexity, hence their reduced-complexity noncoherently detected counterparts might be favored. Finally, we conclude by touching upon the promising research area of quantum-domain communications, which might be expected to circumvent the aforementioned complexity problem of massive MIMOs with the aid of efficient quantum-domain search techniques—a truly exciting research era ahead for wireless researchers.

KEYWORDS | Cellular capacity; cellular systems; channel state information (CSI); design loss; implementation loss; infrared communications; multiple-input–multiple-output (MIMO) systems; optical wireless (OW); quantum communication; Shannon bound; visible light communications; wireless future

I. TRENDS AND MOTIVATION

Since the end of the 19th century, when the feasibility of radio transmissions was demonstrated, mankind has endeavored to fulfill the dream of flawless wireless multimedia telecommunications, enabling people to communicate with anyone, anywhere, at any time, using a range of multimedia services. In fact, "virtually" being with someone, anywhere, at any time at the push of a dialing key—provided that the wireless system, the communicator device as well as the human/communicator interface are up to the associated requirements—is a concept that ultimately leads to the impression of "telepresence" while communicating.

Naturally, the provision of these "telepresence" services requires a further quantum leap from the current state of the art represented by the popular mobile telephone.

A. Wireless Generations

Telecommunications has become one of the most vital enablers of wealth creation. While the proportion of the globe's population, who owns a fixed-line-based telephone remains limited, observe in Fig. 1 that the penetration of mobile phones far outstripped that of its fixed-line counterparts. We hasten to add, however that there is a cohort of subscribers, who rely on several mobile phones, for example for their private and business use. Since the development of wireless communications was recently detailed in [1], in this treatise, we restrict our historical perspective to a rudimentary review of the past and concentrate more on the future.

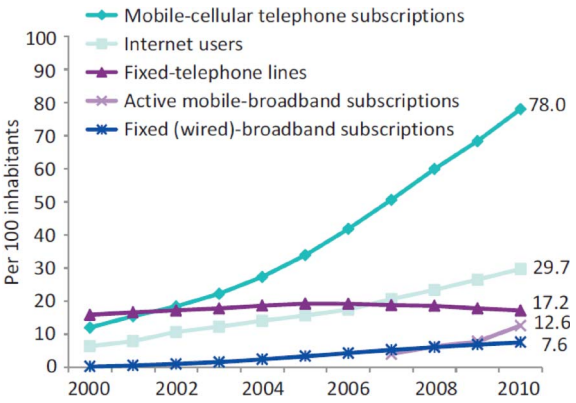

Fig. 1. ***The penetration of the global ICT developments during 2000–2010 (© ITU World Telecommunication/ICT Indicators database [8, p. 1]).***

Naturally, at the beginning of the 20th century, it was only the "rich and famous" who enjoyed the early privilege of tetherless communications. The first land mobile radio system designed for broadcasting messages to police vehicles was installed in 1928, while in 1933, a two-way mobile radio voice system was introduced by the Bayonne New Jersey Police Department. These early mobile radio transceivers used power-hungry valves, since the transistor was not invented until 1947. An early European development was the Swedish Mobile Telephone System A (MTA) introduced in 1957, which had a 40-kg "*mobile*" terminal and supported 125 users until 1967. In 1966, the Norwegian Offentling Landmobil Telefoni (OLT) system was launched, which operated until 1990. The 1980s witnessed the development of numerous national mobile phone systems, most of which relied on analog frequency modulation (FM) and hence were unable to employ digital error correction codes.

The historic developments of the past two decades in wireless standardization are illustrated in Fig. 2. The aforementioned first-generation (1G) systems were all based on analog FM and predominantly operated in the 450-MHz radio-frequency (RF) band. By contrast, the second-generation (2G) systems of Fig. 2 opted for digital modulation techniques and hence had the benefit of using error correction codes, which resulted in a substantially improved speech quality. The countries of the European Union (EU) developed the first digital cellular system during the 1980s, which was later adopted across the globe. Hence, it is referred to as the Global System of Mobile Communications (GSM) [2]. The system supported eight users per carrier with the aid of time-division multiple access (TDMA) in a 200-kHz band. Hence, the cost of the

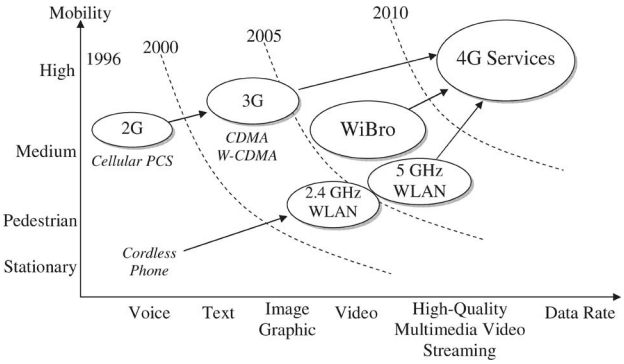

Fig. 2. ***Evolution of standardized wireless systems and of the Wireless Broadband (WiBro) services provided by them portrayed in the mobility versus data-rate plane [9].***

channel units was shared among the eight users per channel. The GSM system was launched in the 900-MHz frequency band, but later it was also rolled out in the vicinity of 2 GHz, where free spectral bands were more readily available. This had the disadvantage, however, because the typical pathloss is higher than say at 900 MHz, for example. Hence, the typical cell size had to be reduced, which made the base-station (BS) infrastructure potentially more expensive, since more BSs were required, even if they were lower power BSs.

In competition with GSM, a number of other 2G digital standards emerged, such as the TDMA Pan-American digital advanced mobile phone system (D-AMPS) and the direct sequence code-division multiple access (DS-CDMA)-based system [3] known both as IS-95 and CDMAone. The IS-95 system also had an evolved counterpart, namely the Pan-American cdma2000 system, which had three parallel CDMA carriers, leading to the first standardized multicarrier CDMA (MC-CDMA) system [3]. This development resulted in a trippled bitrate potential. However, the 2G systems had a low data throughput, which was insufficient for advanced video and wireless Internet services—they were voice and text only systems, as indicated in Fig. 2.

Hence, the research community embarked on the design of higher rate systems with the objective of enriching the range of services offered, which naturally required higher bitrates. Substantial research efforts were invested in defining the third-generation (3G) standard based on wideband CDMA (W-CDMA) [4]. The system had a bandwidth of 5 MHz and relied on a chip rate of 3.84 Mchips/s, where all users transmitted their information bits simultaneously with the aid of their unique, user-specific chip sequences. The 3G systems operate at a RF close to 2 GHz.

It was also realized already during the 2G era that it was unrealistic to expect that any fixed-rate channel coding (CC) and modulation scheme could deliver a time-invariant quality of service (QoS). This realization led to the intensive research of adaptive modulation and coding (AMC)-aided [5] standardized systems, such as the high-speed packet access (HSPA) mode of the W-CDMA 3G systems detailed in [4].

Despite the 40-year research history of orthogonal frequency division multiplexing (OFDM) [6], [7], multicarrier cellular solutions only emerged during the first decade of the 20th century as the dominant modulation technique in the context of the 3G Partnership Project's (3GPP) long-term evolution (LTE) initiative. During this decade, multicarrier solutions have found their way into all the 802.11 wireless local area network (WLAN) standards, which also rely on AMC depending on the near-instantaneous channel quality. Observe in Fig. 2 that the family of WLANs tends to operate at higher frequencies than the cellular personal communications systems (PCS) and this trend continues, since WLAN solutions operating at 60 GHz are also becoming off-the-shelf commodities. Their limitation is however that they only operate reliably in line-of-sight (LOS) scenarios, hence the employment of cooperative solutions circumventing this problem is crucial.

OFDM is also used in the wide area coverage fixed wireless access scheme known as Worldwide Interoperability for Microwave Access (WiMAX) [7]. One of the main benefits of multicarrier solutions is their high grade of flexibility. They have a host of different parameters, which allow us to appropriately configure them and program them, whatever the circumstances are—regardless of both the propagation environment and of the QoS requirements, as facilitated by the employment of AMC.

Casting our eyes back by three decades, since the conception of the 2G GSM system, in excess of three orders of magnitude bitrate improvements were achieved. This impressive development corresponds to an order of magnitude throughput improvement for each of the past three decades, because GSM had a data rate of 9.6 kb/s, while the HSPA system is capable of communicating at 13.7 Mb/s. Without the dramatic advances in both signal processing (SP) and the achievable SP speed, this performance improvement would have been impossible to achieve. It is important to note however that if the energy required for the transmission of a single bit is assumed to be fixed, then the aforementioned throughput improvement would require a 1000-fold transmit power increase, which is clearly unrealistic.

Thanks to the advances of science and technology, fortunately the bit energy required for high-integrity communications has been substantially reduced, but regretfully not by a factor of 1000. In other words, the possible transmit power reductions remained more limited, even when using the most advanced multistage iterative receivers—the required received signal power has not been reduced by as much as a factor of 1000 or 30 dB. This plausible observation motivates the further research of

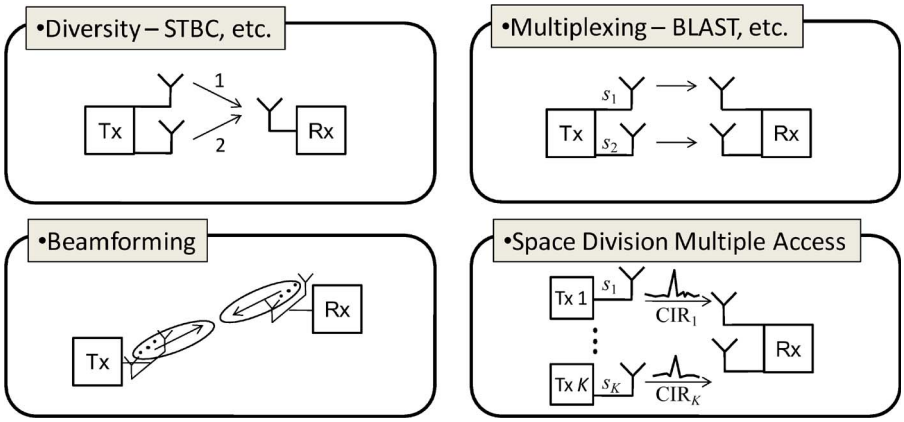

Fig. 3. ***Classification of four MIMO functions [11].***

advanced wireless access, as discussed throughout this treatise, in order to support "flawless telepresence" services.

B. Channel Capacity

Clearly, the increasing smartphone and tablet-computer population resulted in substantial teletraffic growth. It is anticipated that this trend will continue until 2020, since wireless data communications has become the fabric of wealth creation. Its fiscal value is estimated by economists on the basis of predicting how much the economy as a whole would stand to lose in the absence of mobile communications. Given the current level of growth, the data traffic carried by the mobile network in 2020 might be 1000 times higher than that in 2010. As a further challenge, the bandwidth efficiency can only be improved at the cost of reduced power efficiency and *vice versa*, as illustrated by Shannon's channel capacity formula [10]

$$C = f_B \cdot \log_2\left(1 + \frac{S}{N}\right). \tag{1}$$

This equation suggests that while a system's maximum throughput is increased linearly with the bandwidth f_B, it is increased only logarithmically with the signal-to-noise ratio (SNR). Hence, increasing the bandwidth is a more "efficient" technique of increasing the attainable throughput.

C. The Four MIMOs and Their Capacity Enhancements

In contrast to the logarithmic capacity formula (1), the capacity of multiple-input–multiple-output (MIMO) systems was shown to be proportional to the minimum of N_T, N_R, where N_T and N_R represent the number of transmit and receive antennas, respectively. Hence, the MIMO capacity may be deemed to increase linearly with $N_T = N_R$. With the further proviso that the total transmit power is increased proportionately to the number of transmit antennas, a linear capacity increase is achieved upon increasing the transmit power, which justifies the spectacular success of MIMOs. Hence, we may argue that MIMO-aided transceivers and their cooperation-assisted distributed or virtual MIMO counterparts constitute power-efficient *green* solutions.

Depending on the desirable MIMO function to be carried out, MIMO techniques may be classified into four broad categories, such as diversity, multiplexing, multiple access, and beamforming techniques, as shown in a stylized manner in Fig. 3 [1], [11]. More explicitly, these four MIMO schemes were designed for achieving the following four design goals:

- The family of spatial division multiplexing (SDM) [6], [12] schemes of Fig. 3, such as Bell Lab's space time (BLAST) scheme, aim for maximizing the attainable multiplexing gain, i.e., the throughput of a single user. This is achieved by exploiting the unique, antenna-specific channel impulse responses (CIRs) of the array elements for differentiating the antenna-specific MIMO streams, which is reminiscent of the unique, user-specific chip sequences of CDMA.
- Albeit the spatial division multiple access (SDMA) arrangements [6] of Fig. 3 are close relatives of the aforementioned SDM schemes, instead of maximizing a single-user's throughput, they maximize the number of users supported, while sharing the total system throughput among the users supported.
- Alternatively, attaining the maximum possible diversity gain is the objective of the family of space-time block coding (STBC) [13] as well as space-time trellis coding (STTC) [14] schemes of Fig. 3 [15]. They exploit the fact that the MIMO

elements tend to experience independent fading, provided that they are sufficiently far apart. Hence, the chances are that if one of the antennas experiences a deep fade, the others do not.

- Finally, beamforming mitigates the effects of interfering users roaming in the vicinity of the desired user [4], provided that their received signals arrive from sufficiently different angles and hence are angularly separable, as portrayed in Fig. 3.

In practice, the entire propagation and cochannel interference environment is time variant and hence the employment of the multifunctional MIMO schemes would be desirable [1], which might be constructed within a relatively compact space at 60 GHz or a wavelength of 0.5 cm. By contrast, they might only be feasible at say 2 GHz for employment in the BS's downlink transmitter, since at 2 GHz, the wavelength is as high as 15 cm.

D. The Road to Capacity

Over the past 60 years substantial research efforts have been invested in conceiving solutions capable of approaching the capacity—at least under idealized conditions, such as perfect channel estimation, perfect synchronization, arbitrarily long tolerable delays, and unconstrained implementational complexity, just to mention a few.

This process was detailed in the context of both standardized wireless systems and with reference to a range of other potent system solutions, including MIMO systems in [1]. Owing to space limitations, we are unable to repeat all the relevant details here; suffice to say that among others, forward error correction (FEC) coding played a pivotal role in this process [15]–[20]. The aforementioned MIMO techniques were also extended to the family of MIMO solutions relying on the individual single antennas of a number of distributed but cooperating mobile stations "sharing" their antennas in [20], [21]. The design of FEC schemes for cooperative systems requires special attention for the sake of avoiding avalanche-like error propagation owing to the potential decision errors of the relay stations (RSs). Another important design constraint of cooperative systems is that it is unrealistic to expect that, in addition to decoding and reencoding the source's signal, the RS would altruistically also estimate the source-RS channel. Hence, in [21], low-complexity noncoherent detection-aided systems dispensing with channel estimation were conceived.

E. Reducing the Cell Size and Increasing the RF Carrier [2]

As mentioned above, over the years, the cell size of wireless systems has been reduced in an effort to compensate for the increased pathloss, as we moved from the 1G systems operating around 450–900 MHz, then to about 2 GHz, and further to 2.4, 5, and 60 GHz. The attenuation/pathloss versus RF carrier trends are portrayed in Fig. 4 across the range of 10–300 GHz. A further benefit of the cell-size reduction is that the propagation environment

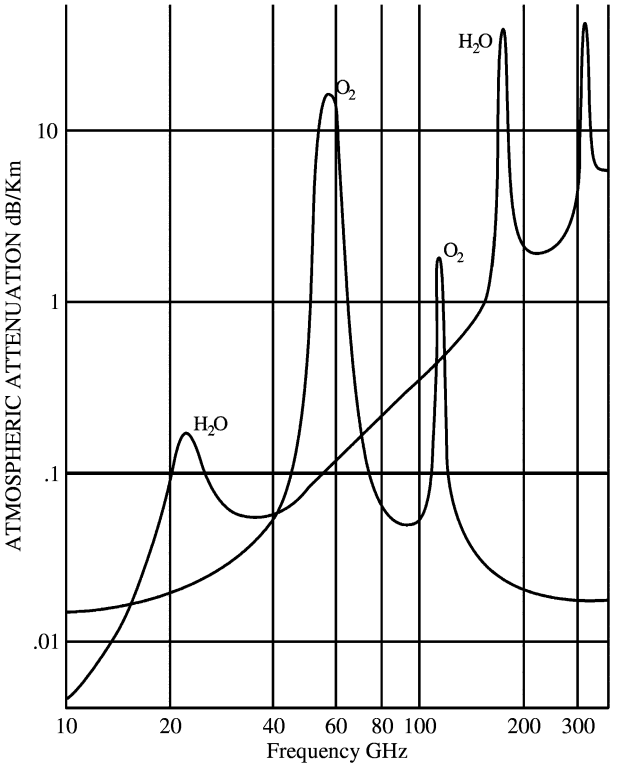

Fig. 4. *Pathloss versus carrier frequency, portraying the typical oxygen and water vapor absorption phenomena [2].*

becomes more friendly, often imposing only a 20-dB/decade pathloss in LOS scenarios, as opposed to the typical 40-dB/decade pathloss of non-LOS situations. As the RF carrier is increased, there is strong experimental evidence that the signals are absorbed by the environment in non-LOS scenarios and hence the employment of the aforementioned cooperative solutions [1], [20], [21] becomes more crucial. Furthermore, since the wavelength at 60 GHz is only 0.5 cm, the "massive" multifunctional MIMO schemes of [1] might be constructed within a relatively compact space, which was less feasible at say 2 GHz, where the wavelength is 15 cm.

Returning to Fig. 4 for the sake of understanding the associated propagation phenomena as a function of the RF carrier, observe that the electromagnetic radiation is partially absorbed at specific frequencies by oxygen molecules in the atmosphere. So-called resonant absorption lines occur in the band 50–70 GHz [22], [23]. They are resolvable at high altitudes where the molecular density is low, but broaden at the Earth's surface, imposing a high pathloss. The RF band spanning from 51.4 to 66 GHz is the absorption band A_1. Another absorption band, A_2, stretches from 105 to 134 GHz. There are peaks in the pathloss owing to water vapor absorption at 22 and 200 GHz. Fig. 4 portrays these oxygen and water vapor absorption curves. We notice that when the absorption in A_1 reaches a peak, the

attenuation due to water vapor is near a minimum [24]. The oxygen absorption is lower in A_2 than in A_1, while the water vapor attenuation is higher. These observations suggest that band A_1 is more suitable for communications than band A_2.

A study [25] of 60-GHz propagation conducted for small cells revealed that even along corridors in buildings, free-space propagation was experienced. Satisfactory coverage was experienced without the need to align the transmitter and the receiver in offices and in lecture theaters of differing constructions. The transmissivity and the reflectivity of various materials were measured in percentages, such as those of aluminium or brass (0.06%, 99%); wood (6.3%, 2%); plasterboard (63%, 3%) and glass (25%, 16%). The attenuation in signal strength was typically 8 dB owing to pedestrians, 10–14 dB due to cars, 4 dB owing to bicycles and motorcycles, and 16 dB for buses, when the measurements were made as they crossed the LOS path between the transmitter and the receiver.

An attractive application for band A_1 is a point-to-point link, where transmitters and receivers are above the height of pedestrians but below the urban skyline. Because of the absorption properties of band A_1, the same frequencies can be repeatedly reused across a city to give numerous point-to-point links [25]. These links can distribute signals to each dwelling, or link femtocellular BSs together. We note that these applications can also use lower frequencies, say 15–50 GHz, since the urban infrastructure will absorb the radiation and allow frequency reuse. 60-GHz transmissions are of particular value when buildings are widely spaced, e.g., in suburbia, since then the oxygen absorption will effectively truncate the path range. A plethora of attractive 60-GHz system solutions were proposed by Rappaport *et al.* [26].

Again, the grave limitation imposed on "flawless telepresence" by (1) is that given a certain total bandwidth of f_B, linearly increasing the channel capacity requires an exponentially increasing transmit power. However, given the logarithmic nature of (1), the large penetration of mobile phones across the globe seen in Fig. 1, the 1000-fold throughput increase of HSPA over GSM, and the 1000-fold increased teletraffic predictions of the next decade, increasing the transmit power is clearly unrealistic in the light of the dramatically increased energy consumption and energy cost trends observed in Fig. 5. Interestingly, however, it was also shown by Shannon [10] that upon increasing f_B toward infinity, the capacity does not tend to infinity. The limit of (1) becomes $C_\infty = 1.45S/N$, which allows a linear throughput increase for large bandwidth with the SNR—an important justification for the beneficial properties of high-bandwidth CDMA, OFDM, and ultrawideband systems.

Our goal in this contribution is hence to seek promising techniques of resolving the aforementioned conflicting design constraints imposed on the flawless telepresence systems of the future.

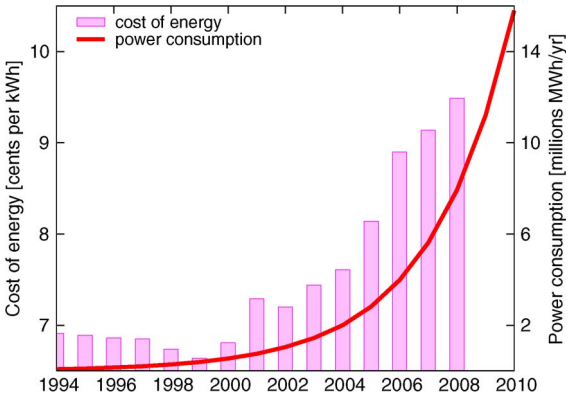

Fig. 5. ***Trends in energy costs and consumption rates over the last two decades [27], [28].***

With this motivation, in the rest of this contribution, we will follow a three-pronged approach.

- First, in Section II, we will quantify the achievable performance of operational wireless systems under both idealized as well as realistic conditions. These deliberations allow us to spot their specific deficiencies in an effort to learn lessons from them in support of future standardization activities.
- In Section III, we will turn our attention to the intricacies of optical wireless (OW) communications, since as seen in Fig. 6, the RF band is rather limited. By contrast, there are significantly broader spectral bands in the optical domain, which could be exploited for high-rate information transmission in support of flawless short-range telepresence services. These advances are expected to become realistic within a decade or so.
- Finally, in Section IV, we provide a rudimentary introduction to the basic postulates of radical quantum-domain communications solutions. Furthermore, we hypothesize that its benefits will lead to off-the-shelf products in the not too distant future—provided of course that the business case is deemed sufficiently convincing to justify the necessary investment into its research.

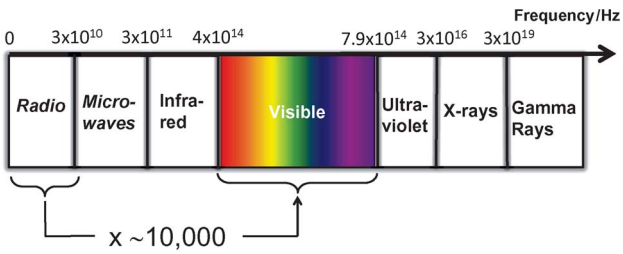

Fig. 6. ***The electromagnetic spectrum.***

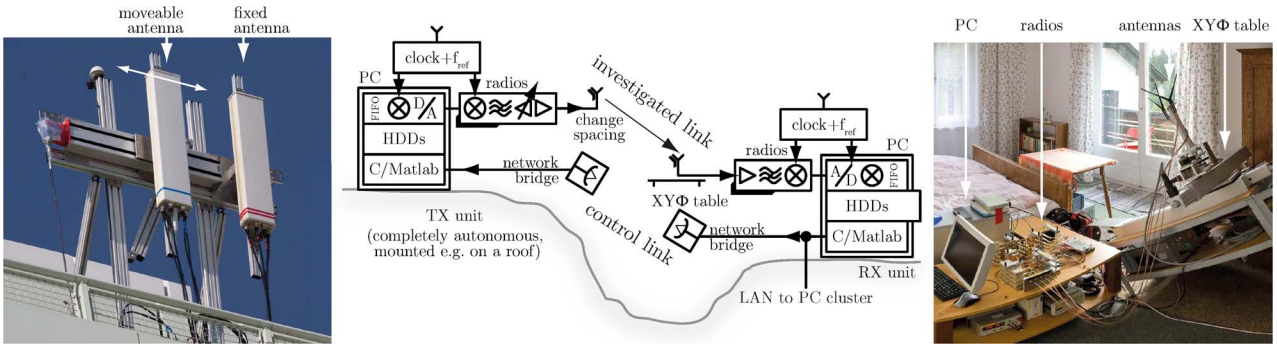

Fig. 7. ***The measurement testbed [35].***

II. PRACTICAL LIMITATIONS OF EXISTING STANDARDS

In this section, we study the true throughput capabilities of the operational 3G and 4G systems. We find that for all systems currently commercially deployed, there is a substantial gap between the Shannon capacity and the throughput measured. The used measurement setup is portrayed in Fig. 7.

A. Cellular Systems Investigated: WiMAX, HSDPA of the HSPA System, and the So-Called LTE System

We analyzed the following three standardized 3G/4G cellular systems.

- The WiMAX [7] physical layer, as defined in IEEE 802.16-2004, Section 8.3: This standard was developed to provide wireless Internet access for stationary and low-mobility users [29]. We studied this system using realistic measurements by employing the OFDM physical layer relying on 256 narrowband subcarriers. By choosing one out of seven AMC schemes at the transmitter, the data rate is adjusted according to the near-instantaneous channel conditions, thereby maximizing the available data throughput. The standard defines various channel codes and we selected the mandatory Reed–Solomon/convolutional code (RS-CC) combination as well as the optional convolutional turbo code (CTC). Furthermore, we designed a regular construction low-density parity check (LDPC) channel code, which is not defined in the standard. Unless stated otherwise, all our results refer to the CTC. In order to utilize transmit diversity, the standard recommends furthermore a simultaneous transmission using two transmit antennas relying on Alamouti's space-time coding scheme.[1]
- The high-speed downlink packet access (HSDPA) mode of the Universal Mobile Telecommunications System (UMTS) [30]: The first version of HSDPA was introduced in Release 5 of UMTS to provide high data rates for mobile users. This is achieved by a sophisticated amalgam of several techniques, such as a prompt link adaptation, hybrid automated repeat request (HARQ) relying on 2-ms minislots,[2] and efficient scheduling. In contrast to the pure transmit power adaptation performed in UMTS, the link adaptation in HSDPA adjusts the data rate by controlling the number of simultaneous spreading codes, the number of bits per symbol, and the channel code rate, depending on the so-called channel quality indicator (CQI) feedback. MIMO HSDPA, standardized in Release 7 of UMTS, further increases the maximum downlink (DL) data rate by spatially multiplexing two independently coded and modulated data streams. Additionally, channel-adaptive spatial precoding is implemented in the DL at the BS, which may simply assign a higher transmit power to one of the antennas, depending on their channel quality. More specifically, this may be activating the best one from a standardized set of power-allocation precoding vectors, based on a so-called precoding control indicator (PCI) feedback received at the BS from the user equipment (UE).
- The LTE [31] and LTE-Advanced (LTE-A) [32] mode of UMTS: While we were able to conduct measurements for characterizing the operational 3G systems, our measurements for LTE have not reached the same maturity, thus we will rely on simulations. To evaluate the throughput of LTE Release 8 and LTE-A Release 9 of UMTS, we

[1]Note that we employed a relatively early version of WiMAX that does not include retransmissions and precoding matrices, which is in contrast to the other two standards considered. However, it turned out during our measurements that such advances have only a modest impact on the throughput observed.

[2]The rationale of using 2-ms minislots is that albeit the system has 10-ms regular slots, retransmitting for example 10-ms speech segments with a 10-ms delay within the next 10-ms transmission frame would be futile, because by then they would become obsolete, since the next 10-ms speech would have arrived.

employed the Vienna LTE-A simulator, which is freely available for academic users [33].[3] We provide simulation results for the (4 × 4)-element MIMO LTE closed-loop and for the (8 × 8)-element LTE-A closed-loop scenarios including the typical performance losses imposed by channel estimation and by selecting the optimal CQI, rank indicator (RI), and precoding matrix indicator (PMI) values.[4]

B. Throughput Bounds and System Losses

In this section, we define several bounds for the achievable data throughput. The differences between the bounds and, eventually, the measured performance may be considered as system losses. More specifically, we will consider three bounds, yielding two differences, plus the difference between the most realistic bound and the measured throughput.

In 1998, Foschini and Gans [36] as well as Telatar [37] extended the Shannon capacity C to MIMO systems. For an OFDM system communicating using a set of discrete subcarrier frequencies[5] $k = 1 \ldots K$, the capacity C expressed as a function of the transmit power P_{Tx}, of the channel matrix $\mathbf{H}_k \in^{N_{\mathrm{R}} \times N_{\mathrm{T}}}$ at the kth frequency bin having a bandwidth of B/K, a total channel bandwidth of B, the receiver noise variance σ_{n}^2, and N_{T} transmit antennas may be shown to be given by [36], [37]

$$C(P_{\mathrm{Tx}}) = \max_{\sum \mathrm{tr}\{\mathbf{R}_k\} \le K} \frac{B}{K} \times \sum_{k=1}^{K} \log_2 \det\left(\mathbf{I} + \frac{P_{\mathrm{Tx}}}{\sigma_{\mathrm{n}}^2 N_{\mathrm{T}}} \mathbf{H}_k \mathbf{R}_k \mathbf{H}_k^{\mathrm{H}}\right). \quad (2)$$

A transmission system that is designed to achieve the channel capacity $C(P_{\mathrm{Tx}})$ of (2) has to perform both frequency-domain and spatial-domain "water-filling"-based precoding according to the matrices $\mathbf{R}_k$, given the realizations encountered. Naturally, accurate water-filling-based precoding is only possible, if *a priori* channel state information (CSI) is available at the transmitter. Hence, we refer to it as CSI at the transmitter (CSIT). Note that the CSI encapsulates both the CIR information and the noise variance or SNR observed at the receiver. Realistically, the CSI can only be estimated at the receiver, resulting in CSI at the receiver (CSIR). This information is then quantized in terms of CQI, PCI/PMI as well as RI and received as CSIT, thus being a crude and outdated approximation of the true CSI. If no CSI is available at the receiver, the best strategy is to transmit the same power from all transmit antennas and over all subcarrier frequencies. The throughput of a system following the latter strategy operating without CSI is bounded by the MI $I(P_{\mathrm{Tx}})$ formula of [36], [37]

$$I(P_{\mathrm{Tx}}) = \frac{B}{K} \sum_{k=1}^{K} \log_2 \det\left(\mathbf{I} + \frac{P_{\mathrm{Tx}}}{\sigma_{\mathrm{n}}^2 N_{\mathrm{T}}} \mathbf{H}_k \mathbf{H}_k^{\mathrm{H}}\right). \quad (3)$$

Note, however, that without CSIT achieving this MI value is beyond our reach, especially because the knowledge of the SNR at the receiver is unavailable. Since the difference between the CSIT-based channel capacity $C(P_{\mathrm{Tx}})$ of (2) and the MI $I(P_{\mathrm{Tx}})$ of (3) is imposed by the absence of CSIT, we define the difference between them as the absolute CSI-related loss $L_{\mathrm{CSI}}(P_{\mathrm{Tx}})$ and the relative CSI-related loss $L_{\mathrm{CSI\%}}(P_{\mathrm{Tx}})$

$$L_{\mathrm{CSI}}(P_{\mathrm{Tx}}) = C(P_{\mathrm{Tx}}) - I(P_{\mathrm{Tx}}) \quad (4)$$

$$L_{\mathrm{CSI\%}}(P_{\mathrm{Tx}}) = 100 \cdot \frac{C(P_{\mathrm{Tx}}) - I(P_{\mathrm{Tx}})}{C(P_{\mathrm{Tx}})}. \quad (5)$$

The above definitions of capacity and MI in (2) and (3) do not take specific practical constraints of the standardized cellular systems into account. For example, the standard systems cannot utilize the entire frequency band and/or the total transmit power for transmitting the original information bits, because a substantial fraction of the spectrum and/or of the transmit power has to be allocated to the pilot, control, and synchronization information. In efficient future systems, the corresponding spectral resource allocation is only justifiable if its effective useful throughput benefits outweigh the required resource investment itself. Suffice to say, in this context, indeed, in low-cost scenarios low-complexity asynchronous and noncoherent solutions might be preferred, as detailed, for example, in [38].

The aforementioned throughput loss imposed by pilots, control, and synchronization information will be

[3]Since its early stages in 2009, we have released the DL simulator in various revision levels and experienced more than 20 000 downloads in the first two years worldwide. Thanks to the multiple responses of our users we continuously improved the quality, so that now it is even being used in the 3GPP standardization. All our simulation results of our publications are also offered for download, supporting a simple means for reproducibility [34].

[4]The RI is an estimate of how many spatial streams can be supported in the DL while the PMI is simply a fixed set of precoding vectors, very similar to the PCI in HSDPA.

[5]We show the formulas in terms of discrete frequency bins $k = 1 \ldots K$, as this is very natural for multicarrier OFDM systems. In HSDPA, an equivalent discrete Fourier transform (DFT) of the CIRs has been applied to calculate the frequency-domain channel coefficients, which in turn are required to compute both the capacity and the mutual information (MI). Since the channels have approximately the same bandwidth, i.e., 5 MHz, the resultant channel capacities match.

accounted for by introducing the measure $I_{\mathrm{a}}(P_{\mathrm{Tx}})$, which we refer to as the achievable MI defined[6] as [43]–[45]

$$I_{\mathrm{a}}(P_{\mathrm{Tx}}) = \max_{\mathbf{W}\in\mathcal{W}} \frac{\beta B}{K} \times \sum_{k=1}^{K} \log_2 \det\left(\mathbf{I} + \frac{\alpha P_{\mathrm{Tx}}}{\sigma_{\mathrm{n}}^2 N_{\mathrm{T}}} \mathbf{H}_k \mathbf{W}\mathbf{W}^{\mathrm{H}} \mathbf{H}_k^{\mathrm{H}}\right). \quad (6)$$

The parameter $\alpha \leq 1$ in (6) accounts for transmit power losses, while $\beta \leq 1$ accounts for bandwidth and transmission time, i.e., time-slot losses. In our setup, we had $\alpha = 1$ and $\beta \approx 0.65$ for WiMAX, while $\alpha \approx 0.4$ and $\beta \approx 0.77$ for HSDPA. For LTE, we found similar values as for WiMAX, albeit β may vary, depending on the operational mode. The precoding matrix $\mathbf{W}$ in (6) accounts for suboptimal precoding/space-time coding. In the case of HSDPA and LTE, the precoding matrix $\mathbf{W}$ is adaptively chosen from a predefined codebook $\mathcal{W}$. Depending on the transmission mode, the inclusion of the precoding matrix $\mathbf{W}$ in the calculation of the achievable MI may or may not (if, for example, the matrices $\mathbf{W}$ are to be unitary) affect $I_{\mathrm{a}}(P_{\mathrm{Tx}})$. Note that in HSDPA a single precoding matrix $\mathbf{W}$ is chosen across the entire bandwidth; LTE, instead, allows for frequency-dependent water-filling-style precoding thereby increasing the achievable MI. In the case of WiMAX, the transmitter employs Alamouti's space-time coding rather than space-frequency coding.[7] In contrast to the CSI-based channel capacity of (2) and the MI of (3) dispensing with CSI, the achievable MI may be interpreted as the practically attainable throughput, constrained by the specific cellular standard.

We define the difference between the theoretical MI $I(P_{\mathrm{Tx}})$ and the achievable MI $I_{\mathrm{a}}(P_{\mathrm{Tx}})$ as a standard-specific design loss, which quantifies the throughput loss imposed by the standardized system design

$$L_{\mathrm{d}}(P_{\mathrm{Tx}}) = I(P_{\mathrm{Tx}}) - I_{\mathrm{a}}(P_{\mathrm{Tx}}) \quad (7)$$

$$L_{\mathrm{d}\%}(P_{\mathrm{Tx}}) = 100 \cdot \frac{I(P_{\mathrm{Tx}}) - I_{\mathrm{a}}(P_{\mathrm{Tx}})}{C(P_{\mathrm{Tx}})}. \quad (8)$$

More explicitly, this design loss accounts for the inherent system design losses imposed, for example, by the transmission of CSI estimation pilots and synchronization symbols, as well as quantized and outdated CSI, rather than perfect precoding, or suboptimal space-time coding. By adapting the design parameters to the specific transmission scenario considered, the design loss may be reduced.

Finally, we define the measurable throughput $D_{\mathrm{m}}(P_{\mathrm{Tx}})$ that may be measured in bits per second for a given link, allowing us to define the so-called implementation loss

$$L_{\mathrm{i}}(P_{\mathrm{Tx}}) = I_{\mathrm{a}}(P_{\mathrm{Tx}}) - D_{\mathrm{m}}(P_{\mathrm{Tx}}) \quad (9)$$

$$L_{\mathrm{i}\%}(P_{\mathrm{Tx}}) = 100 \cdot \frac{I_{\mathrm{a}}(P_{\mathrm{Tx}}) - D_{\mathrm{m}}(P_{\mathrm{Tx}})}{C(P_{\mathrm{Tx}})} \quad (10)$$

as the difference between the achievable MI $I_{\mathrm{a}}(P_{\mathrm{Tx}})$ of (6) and the measured data throughput $D_{\mathrm{m}}(P_{\mathrm{Tx}})$, which accounts for all the losses imposed, for example, by suboptimum receivers including a realistic channel estimator (CE), i.e., CSIR, rather than having perfect CSI knowledge at the receiver and channel decoders as well as the selected channel codes. A more detailed discussion of the individual sources of throughput erosion in WiMAX or HSDPA is provided during our further discourse. In order to complete the picture, we also define the relative effective throughput as

$$D_{\mathrm{m}\%}(P_{\mathrm{Tx}}) = 100 \cdot \frac{D_{\mathrm{m}}(P_{\mathrm{Tx}})}{C(P_{\mathrm{Tx}})}. \quad (11)$$

As expected, combining, i.e., summing up, all the relative losses and the relative throughput results in 100%.

C. Measurement Methodology and Setup

Mathematical models are commonly used for predicting the behavior of man-made or natural systems. We apply mathematical models for weather forecasting and predicting our climate in hundred years and the performance of next-generation wireless systems. Clearly, models reflect the behavior of the system under investigation. Depending on how precisely we know the behavior of a modeled system or subsystem, our prediction models may be more or less accurate. A higher modeling accuracy typically requires an increased number of parameters and complexity. Yet, the beauty of a model lies in its simplicity. If a model contains hundreds of parameters and requires many hours of simulation time for each new parameter setup, it becomes less tractable, hence less attractive. The 3G wireless systems are complex, since they literally rely on hundreds of parameters. The RF propagation channel, which constitutes a significant part of wireless systems, is the subject of intense investigations. Channel models such as that of the Pan-European WINNER Phase 2+ project [46] may contain more than a hundred parameters for the sake of

[6]Note that there exist many different terms in literature describing a constrained capacity; the most prominent ones are spectral efficiency [39], noncoherent capacity [40], functional capacity [41], and classic capacity without CSIT [42].

[7]The terminology of space-time coding entails that appropriately encoded replicas of the signal are mapped to both the time-domain time slots and to the spatial-domain antennas in the interest of achieving independent fading of the signal replicas. This results in a commensurate diversity gain, provided that the channel is nondispersive and hence does not "smear" the orthogonal time-slot signals into each other. By contrast, in case of OFDM modems, often space-frequency coding is invoked, where the signal replicas are mapped to the OFDM subcarriers, instead of time slots.

accommodating a multitude of propagation scenarios with extreme flexibility. If not an expert in modeling, a user may arrive at spurious results, when employing such complex channel models. We therefore based our investigations on accurate and readily repeatable measurements.

Compared to simulations, measurements are tedious. On the other hand, each measurement scenario represents a true, realistic, and physically encountered scenario. When investing further efforts, the measurements may be made repeatable, although not easily reproducible.[8] In order to minimize the measurement errors on the results, we employed rather expensive, self-built bespoke measurement equipment having a high linearity, a large dynamic range of operation, and a low noise figure. In the digital domain, we employed receiver structures having the highest possible performance for real-time implementation. Our linear minimum mean square error (LMMSE) equalizer coefficients were computed using 64-b floating point MATLAB calculations relying on 60 equalizer taps, which result in a significantly higher precision than what we can expect in commercial low-cost fixed-point UEs. In HSDPA, we also applied successive interference cancellation for canceling both the effects of the synchronization preambles and CE pilot signals from the data as well as eight turbo channel decoder iterations in order to attain the best possible results. Due to cost limitations, however, such optimized receivers are unlikely to be employed in commercial 3G systems. Therefore, the measured results accurately quantify the expected performance of commercial systems.

Measurements are realistic, since they exclude idealized simplifying assumptions in general. In a realistic scenario, we do not know, for example, the channel, the frequency offset, or the noise variance, hence this is a natural scenario to be characterized by measurements, but not necessarily by simulations. Severe, realistic, and unknown impairments imposed by unknown sources only occur in practical measurements, never in simulations.

Several practical scenarios have been characterized by our measurements over the few past years, ranging between two extremes: alpine (Carinthian Alps) as well as urban (downtown Vienna, Austria). Further detailed comparisons may be found in [43]–[45], [47], and [48].

The performance of wireless systems is typically evaluated by drive tests, i.e., by continuously measuring the attainable throughput in a vehicle, while driving along a road. Unfortunately, the same test repeated on another day may result in entirely different outcomes. In order to make our measurements repeatable, we applied a measurement technique employing XY positioning tables, where we automatically change the downlink receive antenna positions and characterize many locations in an area of $3\lambda \times 3\lambda$, where the wavelength λ is about 12 cm at 2.5 GHz. Given a specific scenario, at each antenna position, we perform repeated measurements using all transmission schemes of interest. By using this setup, we ensure that all schemes are measured under exactly the same conditions. The measurement results averaged over all antenna positions hence reflect the estimated mean value of the throughput at a given transmit power P_{Tx}. For WiMAX, the channel's coherence time is sufficiently high for measuring all seven AMC modes, one after the other. The receiver later simply picks the best out of the seven measurement results to characterize the maximum attainable throughput. In HSDPA, however, the number of modes is higher and so is the typical vehicular speed. Here, a so-called "mini-receiver" technique was introduced [45], [49], in which a MATLAB routine optimized for execution speed estimates the CQI by computing the post-equalization signal-to-interference-plus-noise ratio (SINR) from the CSIR and feeds it back to the transmitter in the form of the CQI and PCI for generating the CSIT as a crude quantized and outdated estimate of the true CSI.

Similarly, the channel coefficients were also evaluated using the same method. Explicitly, we measure a set of channels at the highest possible transmit power P_{Tx} of 36 dBm and evaluate the channel coefficients by the best CE we have available (LMMSE) utilizing all data, i.e., not only the pilots.[9] This provides us with the highest possible CE quality, which is substantially more accurate than the CE relying on the CE pilots only. In possession of these CEs, we then calculated the channel capacity according to (2) and averaged it, in order to obtain the average channel capacity for a given SNR, which is plotted in Fig. 8. Similarly, we evaluated the MI according to (3) as well as all the other constrained metrics, such as the achievable MI of (6). Additionally, we calculated the 99% confidence intervals to quantify the reliability of our estimates. Taking the measurement associated with the highest SNR and using all data symbols for estimating the channel ensured that the level of observed uncertainty was small. For each measurement point, we computed the 99% confidence interval using the bootstrapping method of [50] and plotted the resultant point augmented by a small tolerance bar seen, for example, in Fig. 8, according to the size of the confidence interval achieved. In fact, most of these tolerance bars only appear as points, indicating our extremely high precision. See [49] for a more detailed description of the employed measurement procedures.

D. Throughput Results

Let us now consider here two sets of results as illustrative examples. In Fig. 8, we depicted our measured results obtained for a (1×1)-element single-input–single-output (SISO) link with 5-MHz bandwidth, when

[8]For simulations, this seems to be a simple task, albeit simulation code is rarely being provided in the SP community and hence reproducibility by other researchers is hampered [34].

[9]This is equivalent to the assumption of using decision-directed CE, but assuming that no decision errors contaminated the detected date.

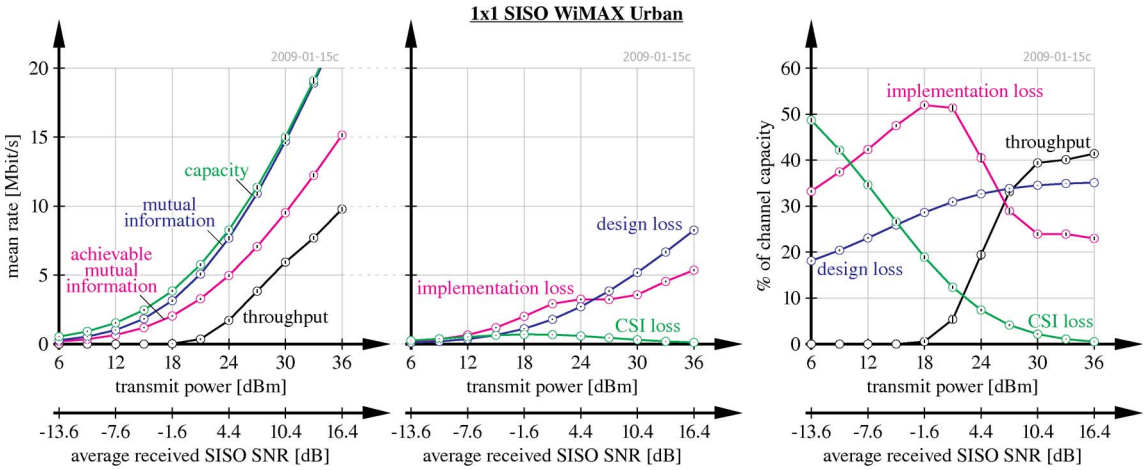

Fig. 8. ***Example of measured WiMAX performance metrics (left) and derived throughput losses, absolute (middle) and relative (right) at 5-MHz urban channel. (Reproduced from [44].)***

transmitting WiMAX signals in an urban environment. We show both the absolute and relative losses for these scenarios. The interested reader will find detailed comparisons of WiMAX and HSDPA in both urban and alpine environments in [43]–[45], [47], and [48]. Additionally, (1 × 1)-, (2 × 2)-, and even nonstandard (4 × 4)-element MIMO-aided HSDPA transmission results can also be found in [43]–[45] and [48].

In Figs. 9 and 10, we portray the absolute throughput values for a (4 × 4)-element LTE system and for an (8 × 8)-element MIMO-aided LTE-A system for transmission in a 5-MHz bandwidth over the pedestrian B channel, respectively. A detailed analysis of the various losses can be found in [45], [51], and [52]. Although different in terms of absolute throughput values, the relative losses of LTE and LTE-A are similar to the corresponding WiMAX and HSDPA results. Note that we did not draw the throughput achieved all the way to its maximum value of 79 Mb/s in LTE and to 158 Mb/s in LTE-A, since an unrealistic SNR of 50 dB would be required. In fact, even the depicted maximum SNR value of 25 dB would be hard to achieve. The assumption of a pedestrian B channel turns out to be quite a realistic model for the urban measurements.

In Fig. 8, all metrics defined in (2), (3), and (6) are shown in terms of both their absolute and relative values for SISO WiMAX transmissions. In the literature, we often find the performance measures defined above to be a function of the SNR at the receiver [31], [53], [54]. However, this approach may be deemed somewhat obsolete. There are at least three reasons for this, the first being that we carry out the measurements by fixing the transmit power P_{Tx} and upon comparing two different systems we

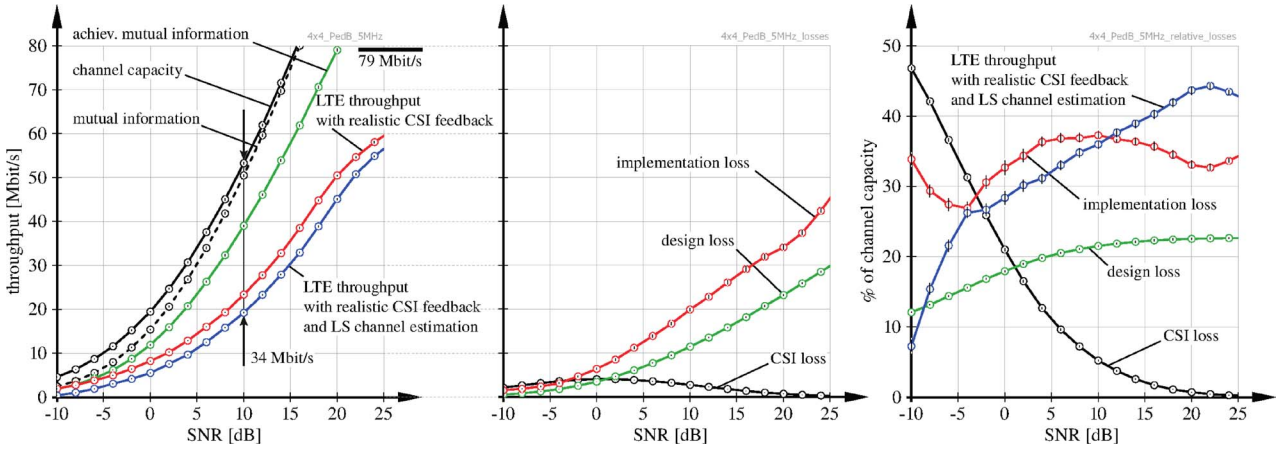

Fig. 9. ***Expected throughput for LTE with 4 × 4 antennas (left) and derived throughput losses, absolute (middle) and relative (right) at 5-MHz bandwidth, pedestrian B channel.***

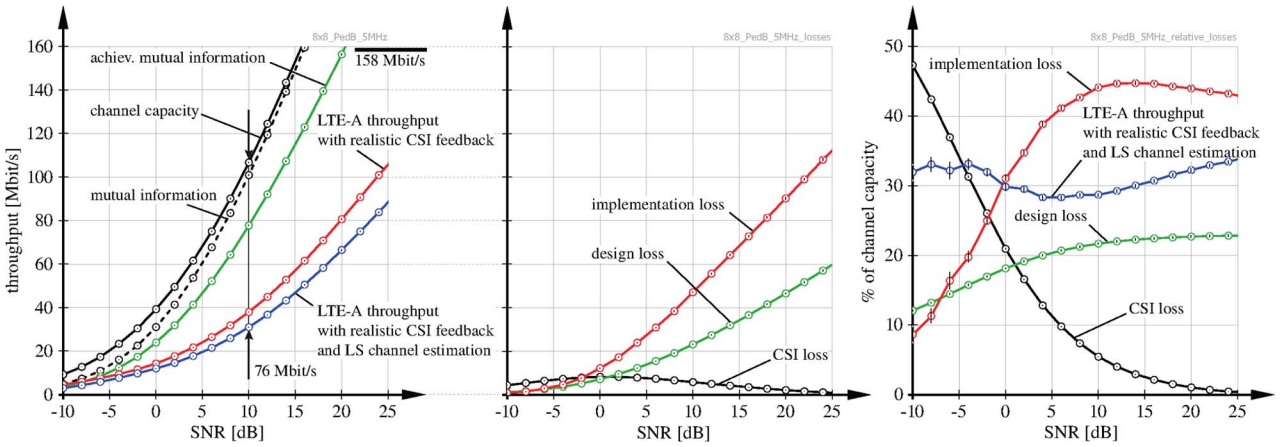

Fig. 10. ***Expected throughput for LTE-A with 8 × 8 antennas (left) and derived throughput losses, absolute (middle) and relative (right) at 5-MHz bandwidth, pedestrian B channel.***

should compare them at the same transmit power, not at the same receiver SNR. Once channel-adaptive precoding is introduced, the received power is effectively increased, also increasing the received SNR without changing P_{Tx}, hence providing a second reason. Third, depending on the scenario and the construction considered, a receive antenna will receive on average a different amount of power than another. These differences might be as high as 6 dB in the mean. The reason for these differences is because the scattering propagation environment is nonsymmetric in nature, as opposed to what has been assumed in most of the earlier MIMO channel models, such as those developed during the COST actions COST 259, COST 273, and COST 2100 [55]–[58]. The Winner Phase 2+ project's channel model [46] is the first one to allow for defining such asymmetries. We thus have to plot our results as a function of the transmit power P_{Tx} rather than versus the SNR. Nevertheless, in order to facilitate comparisons with previous simulation results found in the literature, we provide two scales in our measurement-based plots, one being P_{Tx}, while the other one being the appropriately computed equivalent average SISO receiver's SNR. In case of a SISO receiver, this is simply the average power received over the individual SISO channels. By contrast, for a MIMO receiver, the situation is more complicated, since one antenna may consistently receive less energy than another. Hence, we averaged our results over all individual SISO channels, i.e., over four channels for a (2 × 2)-element MIMO system, for example.

In terms of the individual losses, our findings are summarized as follows.

1) *The CSIT-related loss* L_{CSI}: Comparing the CSIT-related loss to the other two losses in Fig. 8, this may appear to be almost negligible, especially at higher transmit powers and thus at higher SNRs [59]. Note the CSIT-induced relative loss shown in the right picture of Fig. 8; the induced CSI appears to be monotonically decreasing with the SNR above 4 dB. However, at low transmit powers (below, say, 18 dBm) the capacity is low anyway. This behavior is clearly visible not only for SISO transmissions, but also in MIMO scenarios when utilizing polarized antennas [59].This loss, as defined in (5), is due to the absence of perfect CSI at the transmitter, which is entirely independent of the specific standard employed. We thus observe a similar behavior in Figs. 9 and 10. The CSIT related loss is only worth reducing by employing accurate CSI feedback, when the transmission system employs more than two antennas and it is operating at low SNRs. A potential 50% capacity improvement may sound appealing, but we note that the absolute throughput itself remains rather low in the low-SNR regime.
2) *The design loss* L_{d}: The differences between the various standards expressed in terms of L_{d} of (8) are not too pronounced. As shown in Fig. 8, the design loss appears as a monotonically increasing function of moderate steepness with the SNR both in absolute and in relative terms. HSDPA may be deemed to be somewhat better designed and its design loss remains near-constant across the entire SNR range [43]–[45], [48]. In WiMAX, the design loss is low for low SNRs and increases with the SNR [45], [47]. In the case of (2 × 2)-element MIMO-aided WiMAX, this is predominantly caused by the employment of suboptimal Alamouti space-time coding. Precoding is not expected to have an impact on the design loss, since the optimal precoding matrices are unitary and so are the proposed precoding schemes in the HSDPA and LTE standards. Note

that the design loss of the considered LTE scenarios is substantially lower than for the two others (22% versus 35%). The design loss is *the* vehicle of the future, which may be reduced by improvements during the design stage. Once the standard is released, the design loss becomes permanent.

3) *The implementation loss* L_i: In environments associated with a root mean square (RMS) delay spread of say 1.1 μs, the implementation loss of HSDPA is high due to its high self-interference imposed by the CE pilots, while in relatively low-RMS delay spread areas such as the alpine environments associated with 260 ns, the behavior is system dependent. In WiMAX, the different delay spreads have no impact, since the cyclic prefix was selected to be sufficiently high. Both WiMAX and HSDPA suffer from SNR losses of several decibels due to suboptimal CC as well as owing to the CSIR estimation error. The higher number of AMC modes in HSDPA does not directly translate into high-performance benefits compared to WiMAX. In LTE, the implementation loss increases with the SNR, eroding the system's performance, especially at high data rates. Comparing the (8×8)-element MIMO scenario to the (4×4)-element one, we recognize that the situation becomes even worse for a higher number of antennas.

The measured throughput D_m typically increases monotonically with SNR. While the OFDM-based systems WiMAX and LTE require a distinct minimum SNR as shown in Figs. 8 and 9, for which a high-integrity transmission becomes possible at all, the CDMA-based HSDPA system offers low-bit-error-rate (BER) transmissions even for low SNR, albeit at the cost of low data rates [45]. Observe however the remarkable throughput behavior of LTE-A in conjunction with an (8×8)-element MIMO, as shown in Fig. 10. Owing to the channel hardening effect, the lower SNR threshold for which adequate transmissions become feasible has been substantially shifted to the left, hence high-rate transmissions become possible even at low SNR values. After incorporating all the losses, the measured throughput $D_{m\%}(P_{Tx})$ actually observed accounts for 45% of the available channel capacity in the best scenarios at high SNRs, as shown in Fig. 8. While its absolute value D_m increases, the relative throughput $D_{m\%}(P_{Tx})$ in fact degrades, when employing more antennas. For example, a degradation is observed from 40% for the (1×1) SISO WiMAX to 30% for the (2×2)-element MIMO-aided transmission [44], [45]. This effect is clearly visible for both our WiMAX and HSDPA measurements, and it is also expected for LTE, when comparing Fig. 9 with Fig. 10. Note that in both figures the maximum throughput is obtained at extremely high SNRs of around 50 dB. At such high SNR values, the relative throughput is degraded to values below 30%.

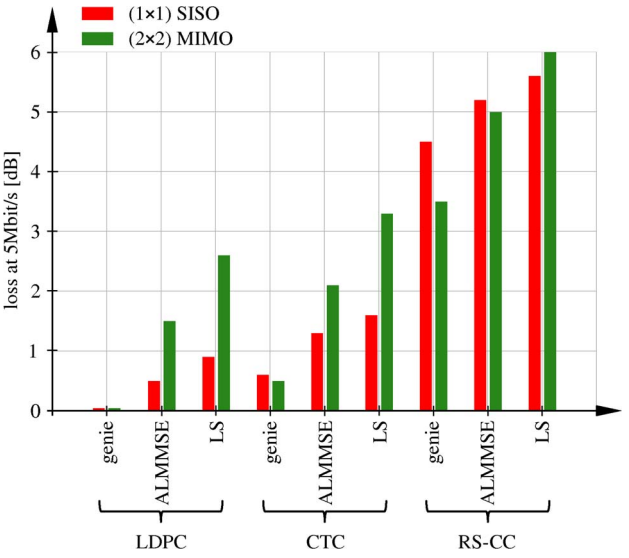

Fig. 11. ***Relative SNR losses of different channel estimators and CC schemes with respect to genie-driven channel estimation and LDPC coding; measured WiMAX in the urban scenario at a fixed throughput of 5 Mb/s.***

E. Sources of Implementation Loss

The implementation loss certainly accounts for many imperfections, for example, phase noise, IQ imbalance, asynchronous timing, and so on. The major sources of this loss were identified to be associated with CC as well as CE. Fig. 11 depicts the SNR loss of various channel estimation and CC schemes at a throughput of 5 Mb/s for WiMAX transmissions when compared to a perfect "genie" channel estimator and LDPC CC. The genie channel estimator is provided with not only the 200 pilot symbols, but also with all the 9400 transmitted data symbols and used them to achieve the highest possible channel estimation quality. Fig. 11 reveals that the difference between the genie-aided knowledge of the channel in combination with high-quality CC on the one hand and realistic least squares (LS) channel estimation combined with the standard mandatory RS-CC channel code of WiMAX on the other hand may be more than 6 dB.

Channel Coding: In the WiMAX measurements of Fig. 8, we employed the standardized RS-CC as well as the convolutional turbo code (CTC). Similarly, a regular LDPC code was designed [47], [49] to provide a high-quality channel code. This code has a variable node degree $d_v = 3$ and has been constructed using the progressive edge growth algorithm [60]. The decoder at the receiver uses the sum–product algorithm [61]. Our LDPC code exhibited a limited SNR loss of 1–2 dB in an additive white Gaussian noise (AWGN) channel, which was also used for selecting the optimal AMC scheme [47], but it was only about 0.5 dB better than the CTC defined in the standard as evidenced by Fig. 11.

Channel Estimation: In Fig. 11, we also characterize various channel estimation techniques. Apart from the simplest LS scheme associated with the lowest complexity, we also implemented an advanced channel estimation scheme, namely the approximate linear minimum mean square error (ALMMSE) technique [62] that improves the LS scheme by taking into account the observed correlation of the subcarriers. Finally, we included the genie-driven perfect CE-based approach, employing all data symbols to provide an upper bound of what might be feasible in the future. In the case of (2×2)-element MIMO transmissions, namely when Alamouti's space-time code is employed at the transmitter, we observe a higher CE-induced performance loss, when we employ the more powerful CTC and LDPC coding schemes. The reason for this is that in the case of Alamouti's space-time-coded transmission, the available transmit power and thus also the pilot signal power are equally shared between the two transmit antennas. Therefore, only half the pilot signal power is available per channel coefficient to be estimated. As a consequence, in a somewhat simplistic, but plausible approach, we might argue that the CE accuracy is at least 3 dB poorer than in the single transmit antenna scenario. Hence, the benefit of the increased diversity is potentially eroded by the loss imposed by the degraded CE. In order to compensate for this effect, one would have to apply a better channel estimator for MIMO scenarios than in the case of SISO transmissions.

Observe in Figs. 9 and 10 that in the HSDPA [45] and LTE scenarios we experience similar effects. Consider, for example, the results of Fig. 9. In the two lower curves (left picture) we characterized the impact of perfectly knowing the CSI versus the estimated CSIR. A CSI-estimation loss on the order of 2–3 dB is common. LTE offers a higher grade of flexibility compared to the previous standards, since it allows, for example, the assignment of (optimal) individual pilot powers to each user. In [63] and [64], the pilot power has been optimized with the aim of maximizing the throughput and, as a results, large SNR-requirement variations (up to 10 dB) were found, depending on the operational mode, on the number of antennas, and on the specific CSI estimation scheme employed.

F. Potential Means for Improvements

What counts at the end of the day when designing a system is the throughput actually achieved. Therefore, a system designer should take *all* losses into consideration, bearing in mind that the design loss imposed by the standardization bodies can never be reduced in the future by sophisticated receiver implementations. Therefore, it is clearly beneficial to standardize systems having a low design loss. As a benefit, when assuming a total affordable discrepancy with respect to the capacity, a low design loss allows us to aim for low-complexity solutions, which may impose an increased implementation loss.

Let us summarize our findings in terms of potential improvements.

- The reduction of the effective useful throughput and the transmit-power loss imposed by the pilots, as well as the CSI estimation error is a substantial source of performance losses. Depending on the specific mode of operation[10] in LTE-A, there may be up to 14% throughput loss owing to the pilots. Since even the best CSI estimate causes losses of 2–3 dB, one may wonder why coherent transmission schemes are considered beneficial at all. For differentially encoded transmission schemes [65], it is well known that typically a 2–3-dB loss[11] is observed compared to coherent detection-aided schemes under perfect CSI knowledge. Thus, low-complexity differentially encoded schemes may offer up to 14% higher throughput at the same SNR.
- In state-of-the-art OFDM-based systems such as LTE, about 25% of the carriers remain unused for data transmission, which allows the system to ensure limited spurious emissions into the neighboring frequency bands in addition to the cyclic prefix overhead, albeit both of these could be potentially eliminated.
- Finally, the huge capacity advantage that MIMO systems offer was eroded in Figs. 9 and 10. Although the (8×8)-element MIMO system offers roughly twice the capacity of the (4×4) MIMO system, the throughput recorded at 10-dB SNR is only about 29% of the capacity of an (8×8)-element MIMO and it is 35% of that of the (4×4) MIMO system. Similar numbers can be deduced for both WiMAX and HSDPA. Thus, upon increasing the number of antennas we employ, the measured efficiency decreases.

Having quantified the practical limitations of the family of existing standardized solutions, let us turn our attention in the next section to a less explored area of wireless communications, namely to the emerging field of OW solutions.

III. INTRODUCTION TO OPTICAL WIRELESS COMMUNICATIONS

Optical wireless communications predates RF wireless by many centuries. Each culture has its own example of using signaling fires to convey the news of an invasion, victory, or other auspicious event. The pioneering work of Gfeller and Bapst [67] in the late 1970s motivated *contemporary*

[10]LTE defines a transmit diversity (TxD), an open-loop spatial multiplexing (OLSM), and a closed-loop spatial multiplexing (CLSM) mode.

[11]Note that often a 3-dB loss is expected which is obtained for a simple differential detection scheme. The optimal maximum-likelihood (ML) decoder [66], however, exhibits only a 2-dB loss.

OW communications research, with the promise of gaining access to thousands of terahertz of bandwidth, which is available in the optical domain of the electromagnetic spectrum. Recall from Fig. 6 the available optical bandwidth compared to the more limited bands available in the RF regions. A substantial—albeit modest compared to RF wireless communications—amount of research on wireless systems operating in the infrared (IR) regions of the optical spectrum has been undertaken. The IR spectral regions used are typically between 800 and 1500 nm in wavelength, with the particular region being a function of both the available components and the encountered propagation environment. A complete survey of this work is beyond the scope of this paper, but the reader is referred to [68] and [69] for further information.

In the past decade or so the employment of solid-state lighting has grown rapidly and in parts of the globe the incandescent bulb has become obsolete—it is no longer on sale. There are predictions that all lighting may be expected to be based on light-emitting diodes (LEDs) in the near future as a consequence of their energy efficiency and reliability compared with the alternatives.

These light sources can be modulated at a higher rate than fluorescent and incandescent sources. Hence, research on using these sources for both wireless communications as well as for advanced illumination is quite active. This research originated in Japan, with the visible light communication consortium (VLCC) [70] playing a leading role. There are already several standards associated with visible light communication (VLC) [71], [72], [73], as well as a growing worldwide research activity. In this section, a brief introduction to both infrared and visible light communications is presented, outlining the prevalent techniques used and the current state of the art. A brief comparison with RF communications is also provided along with a range of key challenges for future research.

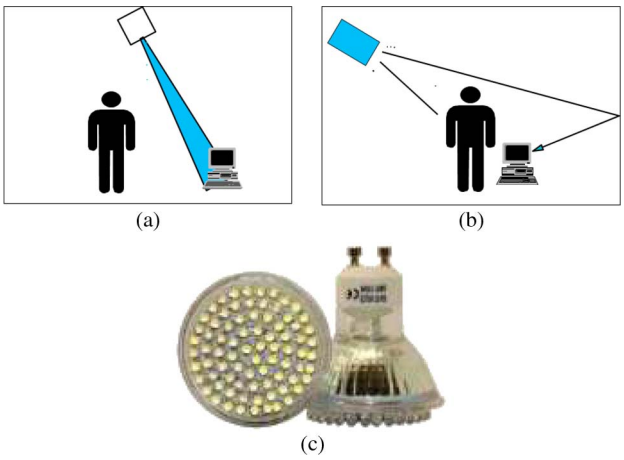

Fig. 12. *Typical optical wireless environment. (a) LOS. (b) Diffuse. (c) LED array.*

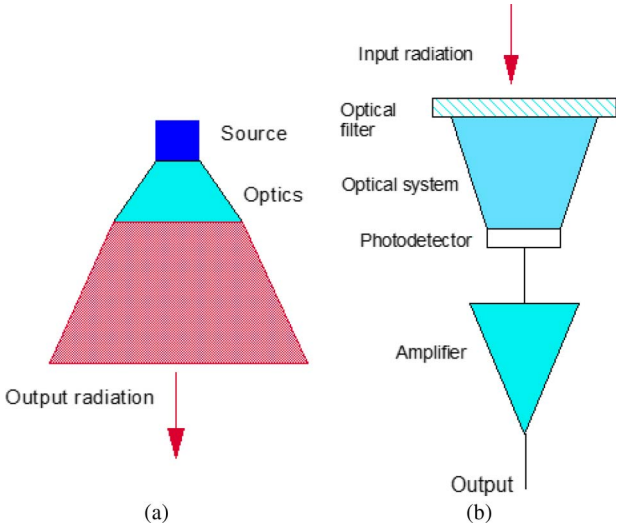

Fig. 13. *(a) Transmitter and (b) receiver components.*

A. Overview of Optical Wireless Communications

Fig. 12 portrays an indoor optical propagation scenario associated with two different OW links. The transmitter consists of a radiating source, whose intensity can be modulated. Light from this transmitter propagates either via a LOS path as shown in Fig. 12(a), or through indirect paths reflected, for example, by intermediate surfaces, as shown in Fig. 12(b). At the receiver, a lens or other optical device focuses or concentrates light onto a receiver. This creates a signal proportional to the optical power incident on it. This is known as an intensity modulation (IM)/direct detection (DD)[12] system, and such channels constitute the basis of the vast majority of OW research. The receiver is effectively an intensity envelope detector, since the optical carrier frequency is 10^{14} Hz, which is too high to be detected using DD receivers.

Fig. 13 shows the schematics of both the transmitter and receiver components, and in the following sections, brief descriptions of each of the components are provided.

1) VLC Transmitter: As alluded to above, LEDs or semiconductor lasers may be used as radiation sources. For these devices, the output optical power is controlled by a drive current, and information is modulated onto their output by appropriately controlling this drive current.

[12]In optical communications, the terminology of direct detection implies that the photodetector directly detects the power of the optical signal. The alternative is coherent detection, where the received signal is optically combined with a reference signal to produce an electronic receiver output signal proportional to the amplitude (rather than power) of the received optical signal. Coherent detection can be achieved either using a local oscillator laser at the receiver, or a delayed copy of the received signal. All this is achieved in the optical domain, using beamsplitters and other optical components.

LEDs are used, where low-cost, high-power sources having modest bandwidths—typically on the order of a few dozen megahertz—are required. For VLC, typically high-power white light sources are used. This light is usually generated by a device that uses a blue LED for exciting a yellow phosphor coating. The yellow and blue lights jointly create the white illumination. The yellow emission has a slow time constant compared to the direct modulation of the blue emitter drive current, hence using only the blue "channel" for communications, and blocking the yellow component at the receiver is a commonly used technique. There is also some work on using red, green, and blue emitters, where an arbitrary color can be produced by modulating the drive currents in each, hence potentially conveying independent information on each of the emitters, or using color to convey information (as set out in the IEEE standard [73], for instance).

Lasers are used in high-performance applications, with most systems operating either at wavelengths between 700 and 1000 nm, where optoelectronic devices are inexpensive, or around 1500 nm, where off-the-shelf devices conceived for silicon fiber optical communications are available and eye safety can be more relaxed. Eye safety may nonetheless remain an issue [74] in the context of lasers (and increasingly LEDs), albeit diffusing elements [75] can be used to make the source safe and to control the emission pattern.

2) Receivers: Fig. 13(b) shows a typical OW receiver. Light enters the receiver through an optical filter. Both natural daylight and artificial illumination sources act as noise sources imposed on the OW signal [76], and the optical filter passes the relatively narrowband radiation of the transmitter, while rejecting the (optically) broadband unwanted light falling outside the useful band. In the case of VLC, the filter is usually used to pass only the blue light from the LED's emission. Light is then focussed or concentrated onto a photodetector using a lens or other optical element. Photodetectors convert the optical power to a current proportional to it. This current is usually converted to a voltage with the aid of a transimpedance amplifier, and then further amplified before data recovery.

The performance of most OW systems is determined by the receiver, rather than transmitter, constraints. For the optical collection element, the aim is to maximize both the field of view, namely the range of incident angles over which the receiver is sensitive to incoming light, as well as the collection area. The product of the aforementioned field of view and collection area is a constant for any optical system [77] (known as the étendue of the system), hence the ability of the system to collect light is directly proportional to the area of the photodetector. However, increasing the area of the detector increases its (electrical) capacitance, which limits the achievable bandwidth. Clearly, the design of OW receivers is subject to a range of complex design tradeoffs, hence it requires substantial further research [78].

3) The Channel: For LOS channels associated with a single propagation path, there are no practical channel bandwidth limitations—the practical limitations are imposed by the design of both the transmitter and the receiver. There are no identifiable interference effects in the context of IM/DD channels even if coherent sources such as lasers are used. Most photodetectors have a diameter of several hundred micrometers (corresponding to hundreds of wavelengths), hence any potential spatial multipath interference effects are averaged by the integrating effect of the photodetector.

By contrast, for non-LOS channels, the intersymbol interference (ISI) due to multipath propagation becomes a problem. In indoor scenarios, most surfaces are so-called Lambertian scatterers, as detailed in [79]. The light incident on them is effectively absorbed and reemitted with equal brightness (as measured by power/solid angle/unit area of the emitting surface) into all angles of emission. This omnidirectional scattering destroys any *knowledge* of the angle of incidence of the radiation onto the wall and the scattering of light by multiple surfaces creates a *diffuse* environment, where a receiver oriented in any arbitrary direction will detect a similar amount of power.

The multiple copies of the transmitted signal impinging at the receiver will have different propagation delays and the power in each of them will be summed/integrated by the photodetector at the receiver. The channel-induced dispersion results in a CIR exhibiting a number of delayed paths, hence its Fourier-transform will have a low-pass nature. The resultant bandwidth limitation may become quite severe. There is a large body of literature that models and measures this dispersion phenomenon (see, for instance, [79]–[81]), but values on the order of a few dozen megahertz are typical for indoor spaces of $5 \times 5 \times 3$ m^3 or so).

B. Link Margins and Channel Characteristics

In OW communications, the relatively poor, compared to RF wireless, link margin has been, and remains, a major challenge. The link-margin scenarios in VLC and IR are different, and are outlined below.

1) Visible Light Communications: In VLC, most spaces will be illuminated by arrays of LEDs installed on the ceiling providing general lighting, and typical illumination levels offer very high SNR. Values of > 50 dB can be achieved at the signal recovery point in the receiver with the aid of low-cost off-the-shelf components [82].

The bandwidth of the propagation space itself is usually in the range of hundreds of megahertz [82], and it is limited by the different LOS path lengths spanning from the arrays of sources to the receiver. The receivers are relatively straightforward to implement at these

bandwidths, hence the LED bandwidth is the major limiting factor. Maximizing the data transmission rate over this high-SNR low-bandwidth VLC channel is a highly active area of research, which is discussed in Section III-C.

2) Infrared Channels: For IR systems, the transmitter power levels are substantially lower than those of VLC and dedicated sources are used. Transmitter powers of a few dozens of milliwatts are typical, with bandwidths of up to a gigahertz (see [83] for an example). The receiver sensitivities are, however, markedly different from those available for RF systems, essentially owing to the employment of noncoherent detection and due to the different noise sources that govern the attainable receiver performance. An optical receiver having a bandwidth of several hundred megahertz, using a sensitive (Avalanche) photodetector might have a sensitivity of ≈ -40 dBm [84], hence a link margin of 60 dB or so would be considered excellent for IR scenarios. This link margin constraint limits the available field of view for a single-transmitter single-receiver link. Modeling studies disseminated in [83] demonstrate that achieving a 15° field of view might be feasible for a 3-m link operating at 1.25 Gb/s, with approximately 30° at 280 Mb/s [84]. The actual values are highly dependent on the specific components and system parameters employed, but broadly speaking achieving data rates in excess of 100 Mb/s with the aid of a single transmitter and receiver remains a real challenge. For the sake of achieving higher data rates, multiple-transmitter, multiple-receiver geometries have been investigated, including what might be referred to as the optical MIMO concepts. These are discussed in Section III-C

3) Modulation: Simple modulation schemes such as on–off keying (OOK) and pulse position modulation (PPM) have been extensively used for OW. The tradeoffs between bandwidth efficiency and power efficiency are different from those of RF systems however, since the optical signal is unipolar. Any bipolar scheme requires the source to be biased with the aid of a direct current (DC) offset, hence the family of more bandwidth-efficient quadrature amplitude modulation (QAM) schemes have a biasing penalty compared to OOK, which to a degree erodes the benefits of QAM schemes. The interested reader might refer to the well-cited book by Barry [69] for an excellent analysis of this.

OFDM has also been extensively studied [85], which was shown to achieve data rates in excess of 500 Mb/s using a single LED [86]. Recently, schemes that use "bias-free" OFDM have also been developed and these strike an attractive bandwidth versus power efficiency tradeoff [87]. For such schemes, the dynamic range and linearity of the emitter devices may limit the achievable performance [88], hence this topic is actively researched for the sake of improving the attainable performance [89].

C. Research Challenges

In the next sections, we detail some of the promising research areas. These are by no means exhaustive, but outline some important areas where future work is required, or areas that are complementary to the RF work outlined earlier in this paper, so that the promise of gaining access to an abundant supply of new bandwidth may indeed become a reality.

1) Optical MIMO: High data-rate OW systems either require multiple transmitters and receivers, or transmitters and receivers that can track each other with the aid of high-gain beamsteering. There are a number of such architectures, including tracking-aided [90], angle diversity assisted [91], imaging-based [92], [93], cellular [94] as well as quasi-diffuse [95], [96] examples. In VLC, multiple LEDs may be used to illuminate the target coverage area with the aid of MIMO-like architectures. This design philosophy is particularly promising for both visible and IR sources, since large arrays of sources/transmitters are relatively straightforward to fabricate. Similarly, receiver arrays constituted by hundreds of detectors become feasible in the interest of constructing massive multifunctional-MIMO (MF-MIMO) systems.

To elaborate a little further, the original RF concept of MF-MIMOs was detailed in [38], where $\lambda/2$-spaced array elements were used for beamforming. Several of these beamformers were incorporated at multiples of the wavelength, so that they experienced independent fading and hence provided a substantial diversity gain. Finally, several of the aforementioned combined beamformer/transmit-diversity schemes were used for the sake of achieving a multiplexing gain. Naturally, the higher is the carrier frequency, the shorter is the wavelength, which would allow us to accommodate the aforementioned massive MF-MIMOs within a confined space with substantial performance benefits, provided that these plausible principles are translated to optical frequencies. Naturally, as a proof of concept, noncoherent detection principles have to be used, but nonetheless, the adoption of this radical concept remains a long-term challenge at optical frequencies. It may be feasible to carry out noncoherent optical beamforming at the transmitter with the aid of a liquid crystal spatial light modulator. Briefly, each pixel may be used as a phase modulator and one may illuminate the entire array with the aid of a plane wave. In a LOS scenario, receiver beamforming may be carried out with the aid of a similar device under certain conditions.

Optical MF-MIMOs hence constitute an attractive research topic of growing interest, particularly for VLC. When each source has a limited bandwidth, the signals of multiple sources may be combined relying on the MIMO concept for substantially increasing the overall data rate [97]–[99]. However, the IM/DD channel does not create a "rich scattering" environment, which would result in a full-rank channel matrix, as typically experienced in RF

wireless communications. In other words, as alluded to earlier, scattering from Lambertian surfaces tends to render the elements of the channel matrix similar to each other, hence no useful angle-of-arrival information is available. Therefore, the related optical MIMO-design issues require further research. Imaging LOS MIMO systems often rely on lenses and other auxiliary elements to create an approximate image of the source array on a detector array [98], [100]. The employment of diffractive elements (that might also be adaptive) to design a particular channel matrix that might be robust to misalignment of sources and detectors, or for the sake of maximizing the attainable capacity, is a current area of research. This shows one of the benefits of optics, in that it is relatively straightforward to shape the optical field, and thus to "engineer" the channel matrix, rather than simply to accept the matrix generated by the "rich scattering" environment.

In this case, the specific choice of the "best" optical elements to use for the sake of achieving the best possible system performance remains an open problem, hence requiring further research. A so-called spatial-modulation-based design alternative proposed in [99] was based on modulating just one out of several MIMO transmitters in isolation, where the index of the activated transmitter itself also conveys implicit information, for example, in case of activating one out of four MIMO elements, it is capable of conveying two bits of information. A particular benefit of this design philosophy is that no MIMO-element synchronization is necessary and that low-complexity single-stream noncoherent detection may be used instead of classic MIMO-style multiple-stream detection. The whole raft of diverse MIMO solutions detailed in [38] and [101]–[103] may also be employed in this OW context, although the unipolar noncoherent nature of the channel is expected to substantially affect the performance of different schemes and their analysis. Therefore, further research is required in order to understand which schemes may be readily translated from RF to the OW domain.

2) Higher Data Rates and Link Margin Improvement: Systems operating at 1.25 Gb/s have been demonstrated [104] and partial link demonstrations also attempted transmission at 10 Gb/s [105], hence high data rates are indeed feasible. Combining these high rates with a sufficiently large coverage area constitutes the major challenge, since the link margin requires a low pathloss for such systems to operate reliably. MIMO-aided systems are indeed capable of mitigating this impediment to a certain extent, but the basic receiver sensitivity is still orders of magnitude worse than for RF. The development of powerful coherent detection schemes is a potential candidate in the longer term; after all, coherent systems are finding favor in high data-rate optical fiber systems, where sophisticated, but increased complexity modulation schemes can be used to increase the achievable spectral efficiency. Parametric amplification[13] has also been investigated [106], as well as optical amplification using fiber [107] and semiconductor [108] amplifiers have been conceived. Both of these require "collecting" the free-space radiation into a waveguide, albeit the loss in achieving this may be almost as high as the gain of the amplifier. Designing high-sensitivity and high-bandwidth receivers is likely to achieve the most significant gains in the near future.

3) Cooperative Optical Communications: Since the predominantly LOS OW systems exhibit a poor performance in the presence of obstructing objects, it is of paramount importance to develop cooperative techniques, which are capable of circumventing the problems imposed by LOS propagation.

The widespread use of wireless fidelity (WiFi) [7] and mobile broadband services means that future OW systems will coexist with established RF communications. How best to use these systems cooperatively is still a relatively open research question. The use of OW hotspots providing very high data-rate connections, combined with RF coverage for reliability, is attractive (and similar to some concepts developed by relying on 60-GHz RF communications) [109]. In the case of VLC, the ability to visually see the hotspots and move toward them is a further advantage. The analysis disseminated in [110] shows that there is advantage even if only an optical "downlink" is available, which shows the potential promise of the technique.

During the early evolution of optical communications even the fastest analog-to-digital converter (ADC) and electronic SP techniques were unable to process high-bandwidth, high-rate optical signals. Hence, relatively unsophisticated optical-domain SP had to be used. However, over the years, both the ADCs and the SP electronics have become significantly faster, hence potentially facilitating the electronic processing of optical signals.

Different forms of RF system cooperation have been extensively investigated, and together with increased SP power these provide a rich "reserve" of potential techniques to apply to RF/OW cooperation. However, the different characteristics of the optical channel have to be taken into account, hence significant research efforts have to be invested in identifying the most promising approaches.

In the context of long-range *outdoor* point-to-point free-space links [known as free-space optics (FSO)] there has been a substantial amount of work on mitigating the effect of weather-dependent attenuation and atmospheric turbulence, which limits their transmission integrity and throughput [111].

[13]In this technique, the information signal is carried on an electrical carrier so the received photocurrent becomes similar to a carrier-based RF signal. At the same time, the bias voltage of the photodetector is modulated at a local oscillator frequency, which modifies the "transfer function" of the detector. The resultant nonlinear interaction between the incoming and local oscillator signals may be beneficially arranged for providing a gain.

Numerous countermeasures, such as adaptive transmissions [112] and diversity combining [113], [114] as well as relaying, have been proposed for OW communications [115]–[118]. More specifically, the performance benefits of multihop relaying for transmission over so-called gamma–gamma fading channels were quantified in [117], while a comparison of amplify-and-forward (AF)-aided as well as decode-and-forward (DF)-aided relaying was provided in [118].

The aforementioned AF and DF relaying techniques [38] are capable of achieving a reduced pathloss owing to reducing the distance between the source (S) and the relay (R), as well as the relay and destination (D). They also achieve second-order diversity, since the SD and RD links tend to experience independent fading. However, these benefits are achieved at a potentially halved throughput, because the source and the relay transmit to the destination in two separate time slots. The problem of halving the effective throughput may be eliminated by network coding in the context of bidirectional relaying, where the idea is that the R transmits the modulo-two function of the information received from both sources. When this modulo-two information is sent to both destinations, they are capable of decoding the remote source's information by exploiting the fact that they are aware of their own information [119]–[122].

The multiple-source cooperation (MSC) philosophy of RF wireless communication was conceived by Shalvi *et al.* [123], while Zhang and Hanzo [124] comparatively studied physical-layer algebraic network coding (PANC) [125] and superposition coding (SPC)-aided communications.

4) Channel Coding for OW Channels: Just to mention a few more important fields of future research, the information theory of OW systems has to establish accurate capacity estimates [126] for the prevalent OW channel types.

For indoor OW, there has been relatively little work on CC, since their design has usually followed optical fiber practices, where the information typically remained uncoded and the systems were designed for an uncoded BER of 10^{-9}. Nonetheless, recently, forward error correction (FEC) coding has found favor in VLC, combined with OFDM modulation schemes [86] using an uncoded BER of $\approx 10^{-3}$. This is likely to be increasingly used, with the availability of low-cost SP.

In indoor OW scenarios, the channel tends to be time invariant, but this is not the case for FSO, where the atmosphere creates time-variant impairments. There have been a number of investigations on the benefits of FEC coding in this context. For example, Anguita *et al.* [127] conceived powerful FEC coding schemes for FSO channels subject to atmospheric turbulence. A punctured LDPC and a raptor code adaptively controlled the transmission rate for accommodating the near-instantaneously fluctuating channel conditions with the aid of a feedback channel. A coded modulation scheme conceived for FSO MIMO systems relying on Q-ary PPM and LDPC codes was investigated in the context of atmospheric turbulence channels in [128].

A sophisticated FEC-coded OFDM scheme was designed for hybrid optical networks by Djordjevic [129], which was constituted by a combination of different single-mode fiber (SMF), multimode fiber (MMF), and free-space optical (FSO) links. The proposed scheme was based on polarization multiplexing and coded OFDM using LDPC codes, which was shown to mitigate the atmospheric turbulences, chromatic dispersion, and polarization mode dispersion (PMD). The 16-QAM system was designed for a data rate of 100 Gb/s, which required a bandwidth of 12.5 GHz.

5) Optical Wireless Networking—A VLC System Design Example: Having reviewed the body of research to be carried out for making OW systems a commercial reality, in this section, we provide a system design study.

Optical propagation naturally creates confined "cells" of coverage, either limited by the beamshape or the walls and partitions within buildings. This may be deemed to be a beneficial property compared to cellular RF communications, since potentially reduced cochannel interference is imposed and hence the same frequency may be used by each transmitter separated into picocells by the partitions. However, this is still a largely unexplored area of research. There has been some work (see, for instance, [130] and [131]) on medium access control and resource allocation, but there are substantial knowledge gaps that must be filled before the resultant heterogeneous networks can be rolled out. Work in [132] has studied the pathloss model within an aircraft cabin by means of a Monte Carlo ray tracing (MCRT) tool that has taken into account the measured reflection properties of the materials used within the cabin. When using this model, it is possible to determine the spatial throughput maps within the aircraft cabin, when having *multiple optical access points* that are distributed above the rows of seats, as depicted in Fig. 14. A direct current optical OFDM (DCO-OFDM) air interface is considered owing to its robustness to the time-dispersive OW channel [133], [134].

a) Transmitter model: Each transmitter unit is constructed from 16 LEDs, as shown in Fig. 15. The LEDs are realistically modeled according to Vishay infrared emitters for the different wavelengths, as specified in Table 1. The circular transmitter array closely approximates an OW access point, which hence has an omnidirectional radiation pattern. Nine such OW access points are distributed in the cabin, as shown on Fig. 14. The light signal's power distribution across the entire cabin is simulated for each transmitter LED. This enables the separation of source powers and thus facilitates the recording of spatial signal-to-interference ratio (SIR) maps, which are required for estimating the spatial throughput distribution across the entire cabin.

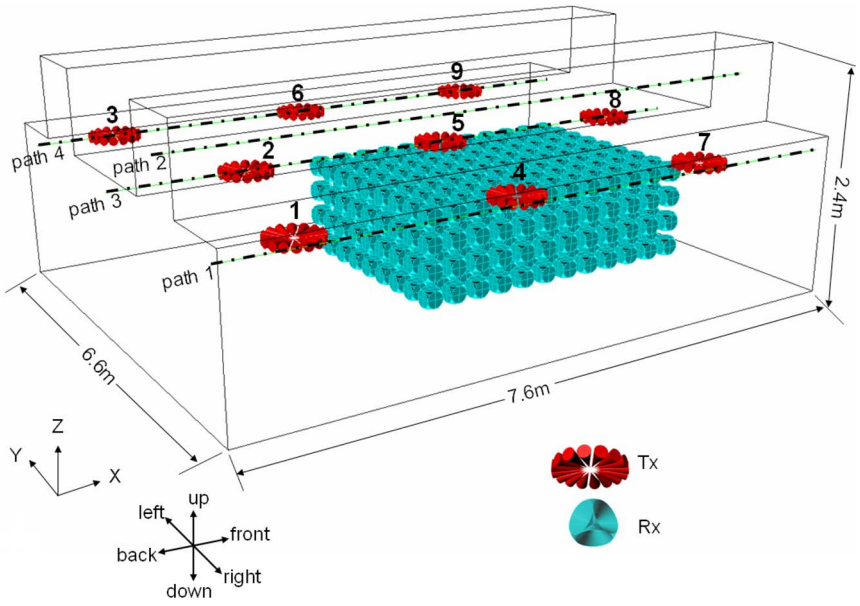

Fig. 14. *The computer-aided design (CAD)-based model of the aircraft cabin. The optical access points are numbered from 1 to 9. The cubes colored in cyan represent the multiple receiver elements for the MCRT tool for an arbitrary snap shot.*

b) Receiver model: The photosensitive area of the photo detectors (PDs) is specified in Table 1. No collimator lenses are considered, but optical bandpass filters designed for the different wavelengths are assumed. A 3-D array of $200 \times 200 \times 100$ receiver units is defined, as illustrated in Fig. 14 with the aid of equidistantly separated irradiance observer planes. Each observer plane is separated from its neighbor by approximately 3 cm in both the horizontal and vertical directions and has a resolution of approximately 3 cm by 4 cm per receiver area. The ray-tracing simulator allows us to separate the signal power received from different directions and thus it is possible to differentiate between the direct path and the multipath reflections arriving at the PD. The goniogram of the LED in combination with the reflection properties of the objects in the cabin determines the power of the direct and multipath components arriving at each PD. Therefore, the radiation pattern of the transmitter unit has a major impact on the signal power distribution in the cabin.

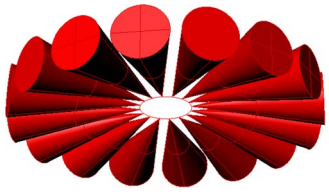

Fig. 15. *Radiation pattern of the transmitter unit. Sixteen LEDs with FOV of $\pm 10^{\circ}$ are placed around a circle with diameter of 2 cm and form an omnidirectional radiation pattern. The transmitter's adequate coverage range determines the size of the resultant optical cell.*

The limitations of the irradiation simulation are related to the stochastic accuracy and the abstraction level of the specific modeling approach invoked. The MCRT simulation stopping criterion of stochastic confidence and the definition of the simulation parameters are of key relevance. The geometric model of the aircraft cabin has a tessellation accuracy related to the resolution of the polygon meshes, which leads to small uncertainties in the MCRT calculation. The reflection characteristics of the materials in the aircraft cabin are defined through measured diffuse and specular reflection coefficients, which are subject to the tolerance of the measurement instruments and setup. The influence of the specific casing geometries of the LEDs and the PDs is not considered. The LEDs are modeled as point sources associated with a specific radiation characteristic and FOV, whereas the PDs are modeled as point receivers with FOV.

c) Determination of SINR: For the given characteristics of the components in the receiver, i.e., PD and transimpedance amplifier (TIA), the electrical AWGN power amounts to -30 dBm. This includes both the thermal and the shot noise at the receiver. Furthermore, a practical BER of less than 10^{-5} is targeted for video broadcast to passenger seats. The network configurations conceived for the different wavelength/frequency reuse factors are presented in Fig. 16. The electrical SINR per symbol at the receiver may be expressed as follows:

$$\frac{E_{\mathrm{s}}}{I+N_0}=\frac{\left(P_{\mathrm{S,opt}}h_{\mathrm{S}}SG\right)^2F_{\mathrm{OE}}}{\left(\sum_i P_{\mathrm{I,opt}}h_{\mathrm{I},i}SG\right)^2F_{\mathrm{OE}}+P_{\mathrm{N,elec}}R_{\mathrm{load}}} \tag{12}$$

Table 1 Front-End Setup

	$\lambda_1 = 830$ nm	$\lambda_2 = 870$ nm	$\lambda_3 = 940$ nm
Transmitter	16× TSHG8200	16× TSFF5210	16× VSMB2020X01
Bandwidth	25 MHz	25 MHz	25 MHz
FOV of LED	±10°	±10°	±12°
$P_{\text{opt,DCO}}$	16× 250 mW	16× 250 mW	16× 250 mW
Receiver	4× S6967	4× S6967	4× S6967
FOV of photo detector (PD)	±70°	±70°	±70°
Area	4× 26.4 mm^2	4× 26.4 mm^2	4× 26.4 mm^2
Sensitivity, S	0.6 A/W	0.63 A/W	0.65 A/W
Capacitance	4× 50 pF	4× 50 pF	4× 50 pF
Bandwidth	25 MHz	25 MHz	25 MHz
Optical filter	4× FB830-10	4× FB870-10	4× FB940-10
Transmittance	0.8	0.8	0.8
Bandwidth	±10 nm	±10 nm	±10 nm
transimpedance amplifier (TIA)	1× AD8015	1× AD8015	1× AD8015
Gain, G	10 kΩ	10 kΩ	10 kΩ
R_{load}	50 Ω	50 Ω	50 Ω
$P_{\text{N,elec}}$	−30 dBm	−30 dBm	−30 dBm
BER	10^{-5}	10^{-5}	10^{-5}

where the electrical symbol power, the total electrical interference power, and the electrical noise power are defined as E_s, I, and N_0, respectively. The same average optical power of $P_{\text{S,opt}}$ and $P_{\text{I,opt}}$ is transmitted by both the serving and interfering transmitters. The radiated average optical power per transmitter of the system is specified in Table 1 as $P_{\text{opt,DCO}}$. Here, the factor h_S represents the path gain between the serving transmitter and the intended receiver, whereas $h_{I,i}$ defines the path gain between the ith interfering transmitter and the intended receiver. The sensitivity of the PD is denoted as S, while G is the gain of the TIA and R_{load} is the resistive load over which the electrical noise power $P_{\text{N,elec}}$ is measured. The optical/electronic (O/E) conversion factor in DCO-OFDM, namely, F_{OE}, can be determined as $(\kappa^2+1)/\kappa^2$, where the signal's standard deviation κ is chosen to bias the DCO-OFDM signal to the positive signal domain [135]. This amplitude shift or biasing into the positive amplitude domain is necessary, because the OFDM-modulated signal has a symmetric distribution across the entire negative and positive amplitude domain, but in the optical domain, we are unable to represent negative signals. In this study, $\kappa = 3$ is considered to minimize the time-domain amplitude-clipping distortion in DCO-OFDM [135].

d) Adaptive modulation and coding: The obtained SINR maps are then transformed into throughput maps by considering a specific AMC scheme. A combination of multilevel QAM (M-QAM) associated with $M = \{4, 16, 64\}$, and adaptive convolutional coding having rates of $R = \{4/5, 3/4, 2/3, 1/2, 1/3, 1/4, 1/5, 1/8\}$, is used. Hence, for the considered bandwidth of 25 MHz, the maximum achievable data rate is 60 Mb/s. In general, for a fixed combination of M and R, the DCO-OFDM system requires $10\log_{10}(\kappa^2+1) = 10$ dB higher SINR for $\kappa = 3$ [135]. The DCO-OFDM system delivers half the throughput compared to an equivalent RF OFDM-based system, since a real-valued modulated signal is required for OW transmission, which requires a Hermitian symmetry in the frequency domain. More explicitly, if the real-valued component of each OFDM subcarrier is the same at both the corresponding positive and negative frequencies, while the imaginary value is inverted, then according to the properties of the Fourier transform, the resultant time-domain signal becomes real valued. Therefore, the SINR requirements for a target BER of 10^{-5} and the corresponding throughput of RF OFDM relying on the AMC of [136] can be used. The DCO-OFDM system is capable of achieving a throughput ranging between 3.13 and 60 Mb/s, over an SINR range between 4.8 and 27.2 dB.

e) Simulation results and discussion: The throughput distribution across the cabin is presented in Fig. 17. Again, it may be observed that DCO-OFDM achieves rates ranging between 3.13 and 60 Mb/s, depending on the receiver's location in the cabin. It is shown that for the stipulated assumptions, the system requires a wavelength/frequency

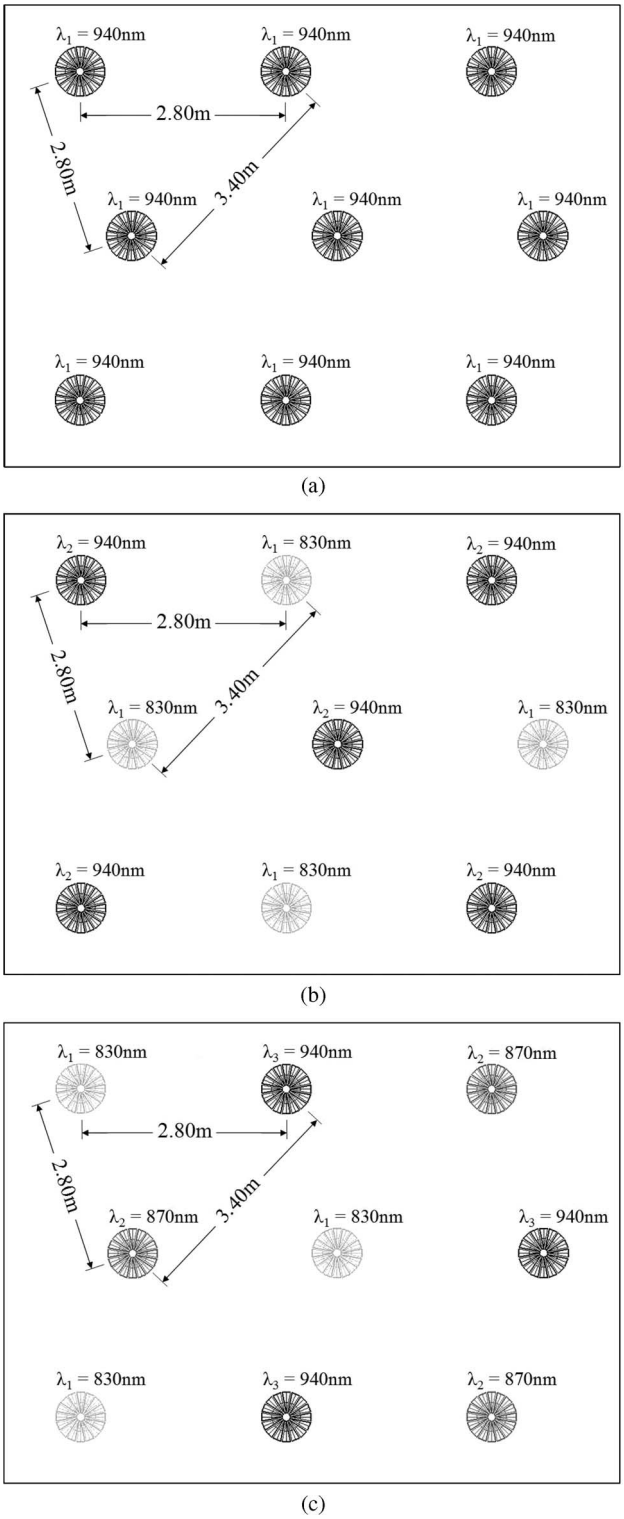

Fig. 16. ***Cell division and wavelength assignment for reuse factors of 1, 2, and 3.***

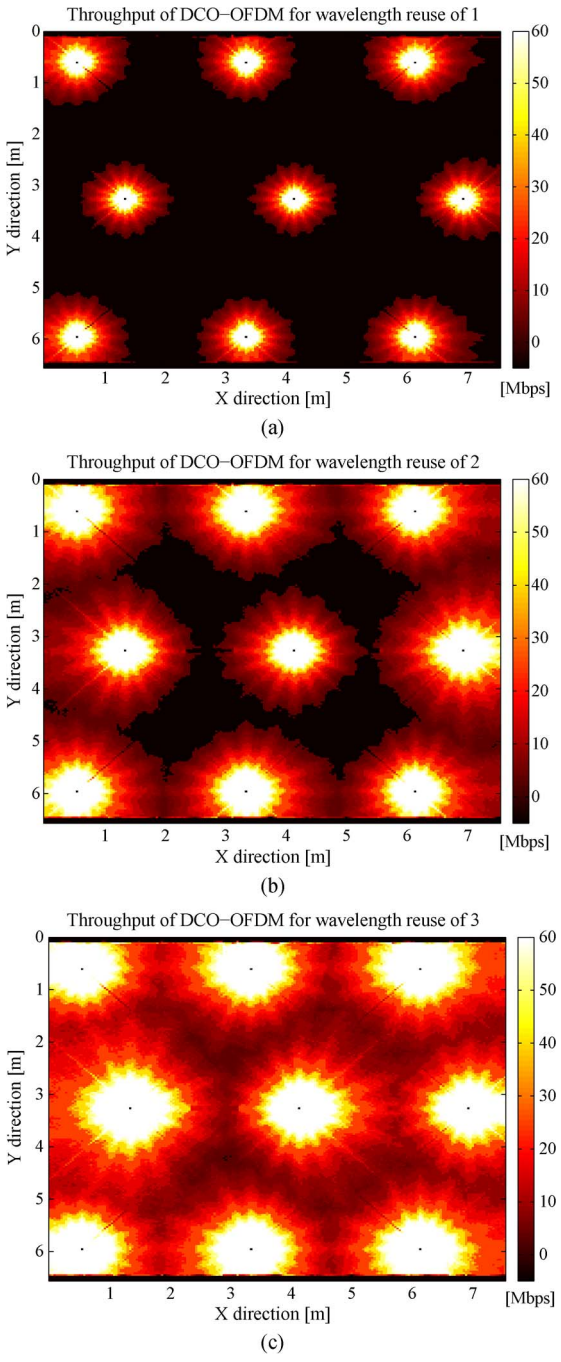

Fig. 17. ***Throughput of DCO-OFDM for wavelength/frequency reuse factors of 1, 2, and 3.***

reuse factor of 3 or higher in order to ensure seamless coverage in the cabin. Interestingly, this agrees with observations typically found in RF-based cellular systems, and it highlights the need for additional research to either exploit the particular properties of optical transmitters and receivers or to use sophisticated interference mitigation techniques similar to the ones used in RF-based cellular systems to arrive at cellular OW systems that allow the employment of a unity frequency/wavelength reuse without significantly compromising the spatial throughput distribution.

Table 2 Comparison of IR and VLC

Attribute	Infra-red	Visible
Infrastructure	Usually requires custom infrastructure (Base Station and Terminal)	Can use LED-based lighting infrastructure
Transmission power	Limited by available sources (10s to 1000s mW)	High modulation power available in a typical room (1-100W)
Channel bandwidth	Can be GHz (limited by channel or transmitter and receiver, depending on type)	10s MHz (set by LED)
Receiver signal to noise ratio (SNR)	Challenging to achieve coverage and good SNR	Standard illumination levels ensure very high SNR (>50dB typically)
Energy in signal	Consists of communications energy only	Significant bias illumination offers potential for self-powered receivers
Achievable data rates	1.25Gbit/s Transport System [104]. Higher rates achieved for links [105] (>10Gbit/s but no coverage)	500Mbit/s data rate (offline) achieved [86].

D. Summary and Conclusion on VLC

Table 2 contrasts IR and OW, while Table 3 summarizes the basic characteristics of OW and shows a comparison between optical and RF wireless systems. The OW research area has benefited from substantial progress over the past few decades, with demonstrations of gigabit per second systems and limited link-level demonstrations at 10 Gb/s. The advent of VLC has opened up new wireless bandwidths, albeit bandwidth that is "owned" by the lighting, rather than the communications provider. OW is potentially attractive as a low-cost "overlay" in the case of VLC where the lighting infrastructure can be reused, and as a high data-rate hotspot-type architecture in the case of IR. In both these cases, it has to be combined with RF wireless solutions in order to provide the best overall network for the user. How these solutions evolve and when OW becomes a commercial off-the-shelf reality clearly depends on the amount of research funding dedicated to this promising research topic. OW uses low-cost electronics combined with complex heterogeneous semiconductor

Table 3 Comparison of Optical and RF Wireless

Attribute	RF wireless	Optical Wireless
Link margin	Excellent, due to coherent detection and noise processes	Poor due to incoherent detection at receiver and noise mechanisms
Signal confinement	Typical propagation loss through walls: 1dB/cm	Confined by internal spaces
Regulation	Subject to licensing and regulation	Subject to eye safety regulation, currently no licensing
Availability of spectrum	Limited and expensive	1000s of THz of spectrum available
Ability to control radiation patterns	Challenging owing to constraints on antenna size in most appliances	High degree of control using lenses and diffractive elements
Propagation	Scattering/reflection and diffraction create broad area coverage	Ray propagation allows very tight confinement of radiation
Interface with fixed network	Need optoelectronic interface of directed RF to connect with fibre network	Possibility of using light from fiber network to create transparent interface

and optical components, whereas in RF communications, the complexity resides in electronic processing. Any future systems have to aim for resolving these difficulties, as well as those imposed by the associated channel characteristics.

At higher carrier frequencies, there may be a "crossover frequency" between their domains, where LOS propagation may be experienced in both cases, hence the associated coverage and blockage issues are expected to be similar, and the electronic convenience of OW is an advantage. It is unclear what this frequency is. A major research challenge for the future is that of improving the link margin, and the conception of techniques for improving the achievable receiver sensitivity, such as, for example, the employment of coherent detection. These coherent techniques are becoming realistic in combination with MIMO-like detection algorithms in high data-rate optical fiber transmission systems. Over the coming decades this should lead to the required drop in component costs, accompanied by a radical increase in processing power, eventually leading to commercially attractive OW solutions.

Holistic OW system feasibility: As discussed in Section II, the scientific and commercial success of RF systems led to attractive services, which substantially contributed to wealth creation. This success, however, led to a paucity of bandwidth in the most benevolent frequency bands below 2 GHz, which motivated, for example, the migration of TV services from the analog band to digital TV to free up the analog TV band. The licence-free, low-power services that may be accommodated in the higher frequency bands spanning from 10 to 300 GHz and seen in Fig. 4 usefully expand the RF coverage into indoor spaces, which may be further extended by the OW solutions portrayed in Section III. These OW systems simply operate by modulating the visible light, hence creating *physically visible OW hotspots*, where the LED transmitters are directly linked together by the mains-power cable. The required power-line communications principles are already well developed and are beyond the scope of this paper. On the other hand, this mains-based linkage of the LED transmitters immediately offers the opportunity of conceiving OW cooperative transmit preprocessing from numerous LED transmitters, with the advantage that there will often be a sufficiently close optical hotspot for supporting OW receivers. The OW hostspots may be expected to spread to street and traffic lights, shops, etc. Naturally, the OW hotspots' teletraffic may also be fed into the asynchronous digital subscriber line (ADSL)-based telephone lines. Alternatively, in the absence of sufficient bandwidth in either the mains/smart grid, in the Ethernet or in the ADSL network, the bitrate will have to be dropped after a seamless handover (HO) to the unlicensed RF hotspots or to the oversailing RF macrocells. The resultant heterogeneous network architecture may be contrasted with the hierarchical cellular structure of the previous generations in Fig. 18, as detailed in [137].

Having reviewed the recent advances in OW communications, let us now turn our attention to the "weird and wonderful" world of quantum-domain communications, where substantial research efforts are required over the

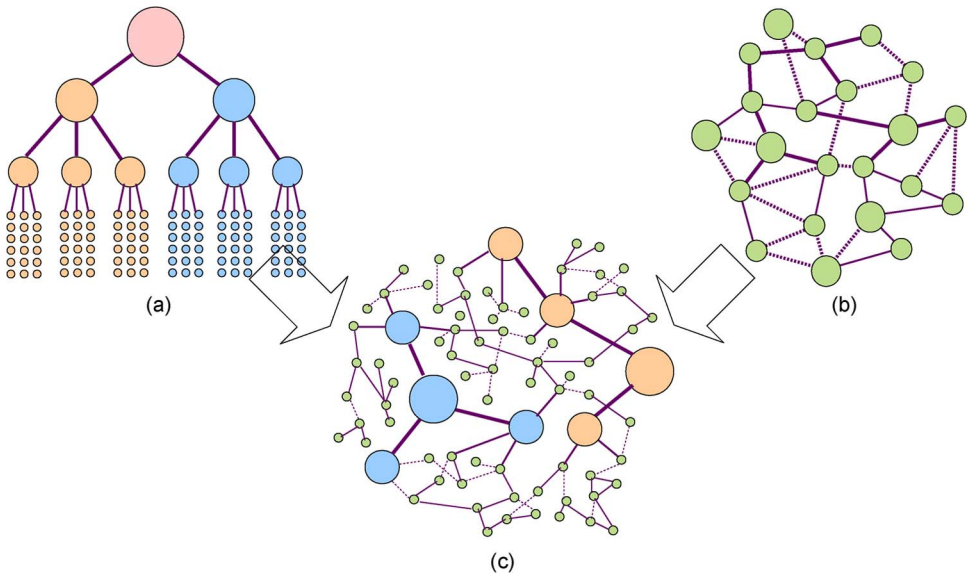

Fig. 18. ***Network architecture. (a) Cellular: scalable and highly dependable architecture used in existing systems; the mobiles communicate with the base stations (BSs), which are under control of the mobile switching center. (b) Ad hoc: flexible, self-organizing architecture. (c) Heterogeneous: a fusion of cellular and ad hoc architectures, showing the licence-free OW/RF hotspots, which hence inherits the advantages of both the cellular and ad hoc topologies [137].***

next decades for making flawless holographic telepresence a reality.

IV. QUANTUM-ASSISTED AND QUANTUM-BASED SOLUTIONS IN WIRELESS SYSTEMS

One day in 1965 when Gordon Moore from Intel was preparing a presentation and started to draw a plot about the performance of memory chips, he suddenly observed an interesting rule of thumb, which was later termed as Moore's law. He concluded that since the invention of the transistor the number of transistors per chip roughly doubled every 18–24 months, which eventually resulted in an exponential increase in the computing power of computers. Although this was an empirical observation without any theoretical substantiation, Moore's law seems to have maintained its validity over the years, provided of course that sufficient investment in science and technology is attracted by the semiconductor industry.

The growth in the processors' performance is due to the fact that we put more transistors on the same size chip. This requires smaller transistors, which can be achieved if we are able to draw thinner lines onto the surface of a semiconductor wafer, lines that are significantly thinner than hair. Current semiconductor technology also enables us to remove or retain certain parts of the wafer according to the specific layout of transistors, diodes, external pins, etc. If the current trend of miniaturization continues, the aforementioned lines will depart from the well-known natural environment obeying the well-understood rules developed step by step during the evolution of the human race and enter into a new world, where "the traveler has to obey strange new rules if he/she would like to pass through this nanoworld." The new rules are explained by *quantum mechanics*, and the "border between these two worlds" lies around 1-nm thickness (10^{-9} m). These rules are sometimes similar to their classic (i.e., macroscopic) counterparts, but sometimes they are quite strange. The reality is though that we have entered this "nanoera," hence we have to accept its rules as the new framework of computing and communications. Let us briefly explore their benefits.

A. Background

In 1985, Feynman suggested a new straightforward approach [138]. Instead of regarding computers as devices operating under the laws of classic physics, which is a common sense, let us consider their operation as a special case of a more general theory governed by quantum mechanics [139]. Our goal is that of seeking algorithms, which are more efficient than their best classic counterparts, but are only available in the quantum world. The corresponding software-related efforts are in the realms of *quantum computing* [140]. We might also hypothesize that the capacity of a *quantum channel* could exceed that of classic wireless links or that we could design more secure protocols than the currently applied ones. *Quantum communications* [141] or *quantum information theory* [142] aims for answering these questions.

In order to understand how quantum computing and communication might improve the performance of our classic wireless systems, let us summarize the four basic rules (called postulates) of quantum mechanics from a telecommunications engineering point of view [140]. These are similar to the Euclidean axioms of geometry in the sense that there are no formal proofs supporting them, but as a difference, anyone who presents an experiment, which contradicts the postulates, might stand a chance of receiving the Nobel Prize. We will demonstrate that any reader who is well versed in wireless communications has sufficient background to accept these rules at an abstraction level, which is required to absorb the results presented in this paper.

In order to pave the way further, we will invoke the well-known DS-CDMA maximum-likelihood multiuser detection (ML-MUD) example as a bridge between the classic wireless and the quantum world.

In our fairly simplified model, the ith symbol of the kth ($k = 1, 2, \ldots, K$) user is denoted by $b_k[i]$, where the symbol duration is T_S. For the sake of simplicity, we opt for the binary phase-shift keying (BPSK), i.e., we have $b_k[i] \in \{+1, -1\}$. The channel-induced signal distortion from the kth user's perspective is modeled by means of $h_k(i,t) = a_k[i]\delta(t - \tau_k)$, where we have $a_k[i] = A_k[i]e^{j\alpha_k[i]}$ and $A_k[i]$, $\alpha_k[i]$ as well as τ_k are typically independent random variables. Finally, $s_k(t)$ refers to the unique, user-specific DS-CDMA signature waveform.

The complex baseband equivalent representation of the signal received at the BS is calculated by convolving the channel's input with its impulse response in the following manner:

$$r(t) = \sum_{k=1}^{K} h_k(i,t) * v_k(i,t) = \sum_{k=1}^{K} a_k[i]b_k[i]s_k(t - iT_S - \tau_k). \quad (13)$$

Since in the uplink different τ_k delays are considered, owing to the different distances of the MSs from the BS, the system is *asynchronous*. Furthermore, $a_k[i]$ is assumed to be completely unknown at the receiver, hence we have to solve a *blind* MUD problem.

When applying matched filters (MFs) in the BS's detector, their output for the ith symbol may be denoted by $y_k[i]$

$$y_k[i] = \int_{iT_s}^{(i+1)T_s} r(t)s_k(t - iT_s)\,dt. \quad (14)$$

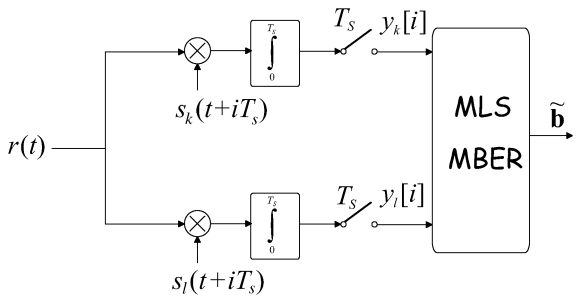

Fig. 19. ***Multiuser DS-CDMA detector.***

In order to formulate the detection cost function (CF) more explicitly, we construct two matrices from the transmitted symbol combinations and from the corresponding MF outputs, yielding $\mathbf{b} = [b_1, b_2, \ldots, b_K]$ and $\mathbf{y} = [y_1, y_2, \ldots, y_K]$, respectively.

To expound further, given the received signals encapsulated in the MF output vector $\mathbf{y}$, we have 2^K different hypotheses according to all the different legitimate transmitted signals hosted by the vectors $\mathbf{b}_m$, yielding the vector $\mathbf{y} = w(\mathbf{b}_m)$ hosting all the received signals. The vector-to-vector mapping function $w(\cdot)$ represents the MFs outputs in response to the transmitted symbol vector $\mathbf{b}_m$ containing the symbols transmitted by all the users. More explicitly, this represents the mth hypothesis. The corresponding MUD architecture is depicted in Fig. 19.

Obviously, $w(\cdot)$ depends not only on the transmitted symbols of the K users, but also on the random channel parameters. Moreover, the mapping $w(\cdot)$ is not reversible. Therefore, we are unable to unambiguously identify that particular transmitted symbol vector $\mathbf{b}$, which results exactly in the received symbol vector $\mathbf{y}$. Instead, the optimal decision relying on the maximum-likelihood sequence (MLS) CF "simply" requires us to spot that particular hypothesis m, which maximizes the conditional probability density function (pdf) of

$$\tilde{b}_{\text{MLS}} : \max_m f(\mathbf{y}|\mathbf{b}_m). \tag{15}$$

1) The first postulate declares how to describe the state of any physical system.[14] To elaborate a little further, a single qbit may be represented as $|\varphi\rangle = a|0\rangle + b|1\rangle$, where $|\rangle$ is referred to as the Dirac's Ket notation [143] routinely used in quantum-physics for describing a state, while a and b are complex-valued numbers satisfying $|a|^2 + |b|^2 = 1$. Hence, the qbit may be interpreted as a vector in the 2-D complex-valued vector space, where a and b are the complex-valued probability amplitudes within the orthogonal bases $|0\rangle$ and $|1\rangle$ of the vector space $|\varphi\rangle$. Considering our ML MUD problem, similarly to the classic vectors $\mathbf{b}$ or $\mathbf{y}$, a quantum register consisting of K qbits stores 2^K legitimate states at any instant, but the quantum register may assume all these states simultaneously, i.e., in parallel, which is formulated as [141]

$$|\varphi\rangle = \sum_{i=0}^{2^K-1} \varphi_i |i\rangle. \tag{16}$$

This implies from our MUD perspective that a single quantum register is capable of storing all the legitimate $\mathbf{b}_m$ hypotheses.

2) The second postulate is related to the time evolution of any system in time domain.[15]

The parallel processing capability of the quantum search originating from the second postulate allows us to find the discrete pdf given by the relative frequencies of those transmitted signal vectors $\mathbf{b}_m$ that lead to a certain received signal vector $\mathbf{y}$, which are then combined by weighting with the corresponding *a priori* probabilities. Finally, in possession of the function $f(\cdot|\cdot)$, we may opt for using quantum search for finding the most likely transmitted signal vector $\mathbf{b}_m$, given a specific received signal vector $\mathbf{y}$.This postulate is one of the key features responsible for the significant speedup of quantum algorithms. Similar to the classic algorithms, any quantum-domain algorithm, such as a unitary transform, can be decomposed into a set of 2-D and 4-D unitary transforms (like the Karnaugh method in classical systems) and implemented by means of a predefined set of corresponding elementary quantum gates. Returning to our ML MUD example, as any classic detector, this ML MUD may be implemented using adders, multipliers, inverters, logical NAND, etc. By analogy, provided that we can find an efficient quantum MUD algorithm, we will be able to implement it using basic quantum gates and circuits. This analogy might appear to be trivial in the light of our everyday practice, but owing to the strange rules of quantum mechanics,

[14]In quantum computing, a quantum bit (qbit) is a unit of quantum information, namely the "quantum" counterpart of the classic bit. More explicitly, the qbit is described by a specific quantum state in a two-state quantum-mechanical system, which is formally equivalent to a 2-D vector space defined over the complex numbers. A specific example of a two-state quantum system is constituted by the two legitimate polarizations of a single photon, namely, the vertical and horizontal polarizations. In a classic system, a bit would have to be either a logical "one" or a logical "zero," but apart from "one" and "zero," quantum mechanics allows the qbit to be concomitantly in a superposition of both states, which inherently facilitates their parallel processing. This beneficial property is inherent in quantum computing.

[15]From an engineering point of view, the Schrödinger equation simplifies to the following essence: the evolution of any closed physical system may be characterized with the aid of unitary transforms obeying the property of $U^{-1} = U^{\dagger}$, and $|\psi\rangle = U|\varphi\rangle$, where $U^{\dagger}$ denotes the complex conjugated and transposed version of U.

it is not trivial at all; quite the contrary, it is remarkable.

3) The third postulate connects the nano as well as the classic macroscopic world and it is referred to as "the measurement."[16]

   From an ML MUD's perspective, the received signal vector $\mathbf{y}$ is entered into the quantum detector, which also prepares an additional register containing all legitimate hypotheses $\mathbf{b}_m$ associated with uniformly distributed coefficients according to the first postulate. Hence, if we performed a measurement on this register, we would find that any of the hypotheses $\mathbf{b}_m$ has a probability of $1/2^K$. The second postulate enables us to modify these coefficients in such a way that the most likely hypothesis will have the largest coefficient. An appropriately constructed measurement will deliver this particular hypothesis with a probability that is proportional to the absolute squared value of the largest coefficient. In order to increase this probability toward unity, we have to conceive a sophisticated quantum algorithm and prepare an appropriate measurement.

4) The fourth postulate defines the technique of combining individual quantum systems. In our ML MUD example, the quantum register containing the hypotheses $\mathbf{b}_m$ has a length of K qbits. It may, however, also be viewed as being constituted by K independent qbits. This postulate sets out the rules of how to switch between the aforementioned two different perspectives. Furthermore, if we would like to combine two detectors, each designed for K users, this postulate outlines how to construct the register having a length of $2K$ in the resultant joint detector.[17]

In conclusion of the basic rules, we emphasize that classic physics and engineering may be regarded as a subset of quantum theory. More explicitly, the postulates discussed above extend the design space of practical algorithms and protocols we may invoke in telecommunications problems. However, this new quantum world simply opens up new realms of solutions, without actually telling us how to construct these solutions. In this respect, its role is reminiscent of Shannonian information theory—it took our community over half a century to find near-capacity solutions capable of approaching Shannon's visionary predictions.

Before delving into any further discussions on quantum-communication-based solutions conceived for future wireless systems, one of the interesting but strange consequences of the above postulates should be mentioned.

- The *no cloning theorem* [141] of quantum computing claims that only known and/or orthogonal quantum states can be copied. Fortunately, classic states, which are widely used in operational computers and processors, are orthogonal, therefore the quantum description of nature as a whole is in harmony with our everyday experiences. This property is useful, if someone would like to protect his/her information against eavesdropping in the communication channel. In simplified terms, we could argue that it is sufficient to encode the classic information states into nonorthogonal quantum states, and as a result, the malicious hacker will become unable to make a copy. However, the *no cloning theorem* imposes a strict limitation, when constructing ML MUD detectors. For example, if we have an inner quantum state computed within the MUD algorithm, it is impossible to make several copies of it in order to perform different calculations on them. One of the most important current research challenges is that of designing repeaters for large wireless and optical quantum networks.
- *Entanglement* [140]: Let us now investigate further what is encapsulated in the notation $|\varphi\rangle$. As argued in [140], when we consider a two-qbit quantum state formulated as $|\varphi\rangle = a|00\rangle + b|11\rangle$, the question arises whether it might be possible to decompose it into two individual single-qbit states, such as

$$\begin{aligned}|\psi\rangle &= (a_1|0\rangle + b_1|1\rangle)(a_2|0\rangle + b_2|1\rangle)\\ &= a_1a_2|00\rangle + a_1b_2|01\rangle + b_1a_2|10\rangle + b_1b_2|11\rangle. \quad (18)\end{aligned}$$

  The answer to this question may be shown to be *no*. To elaborate a little further, a latent linkage exists between the two qbits, and hence, if we decided to measure or determine the first qbit of this two-qbit

[16]Any quantum measurement may be described by means of a set of measurement operators $\{M_m\}$, where m stands for a legitimate classic integer result of the measurement. Quantum measurements differ in two aspects from classic ones. First, they are random in the sense that getting the specific result m has a certain probability. Second, the measurement itself typically influences/perturbs or modifies the measured object. The role of the measurement may be deemed to be analogous to that of the digital-to-analog (D/A) converter in the classic "analog-to-digital (A/D) converter, digital signal processing (DSP), D/A converter" chain. More explicitly, in quantum processing, we have a classic-to-quantum (C/Q) domain converter, followed by a quantum algorithm and a quantum-to-classic (Q/C) converter, where again, the latter block carries out the measurement.

[17]Individual qbits have to be combined by means of the tensor product denoted as $\otimes$ exactly in the same manner as in the case of classic bits (e.g., $0 \otimes 1 \Rightarrow 01$). When considering several qbits, such as for example a two-qbit system, there are four quantum states, i.e., $|00\rangle$, $|01\rangle$, $|10\rangle$, and $|11\rangle$, which are constituted by the tensor product of the first and second qbits. The superimposed state is then formulated as

$$|\psi\rangle = a_{00}|00\rangle + a_{01}|01\rangle + a_{10}|10\rangle + a_{11}|11\rangle \quad (17)$$

where $|a_{ij}|^2$ is the postmeasurement probability of occurrence of the state $|ij\rangle$ normalized as $\sum_{i,j}|a_{ij}|^2 = 1$. Recall that a tensor product may be viewed as a bilinear operator, which is a function that linearly combines the elements of two vector spaces to generate an element in a third vector space, as exemplified by a matrix multiplication.

register, then either $|0\rangle$ or $|1\rangle$ will be obtained randomly with the corresponding probabilities of $|a|^2$ and $|b|^2$, respectively. Provided the measuring equipment observes 0, then the measurement of the second qbit can only lead to 0. Similarly, if the first qbit is 1, the second qbit will also be 1. This is because our two-qbit system $|\varphi\rangle$ contains the superposition of two classic basis states and the measurement is only capable of opting either for $|00\rangle$ or for $|11\rangle$. Plausibly, for $|\psi\rangle$ having four basis states, any combination of 0 and 1 may be encountered. Hence, it appears as if there was a mysterious connection between the two qbits, and indeed, there is. Carefully designed experiments based on the Bell inequalities of [144] or on the inequalities formulated in [145] have demonstrated that this interesting effect remains valid even if the qbits of $|\varphi\rangle$ are delivered to two arbitrarily distant locations. Furthermore, surprisingly, the propagation of this linkage between the two qbits after the first measurement takes zero time.Let us now introduce some further related terminology. The quantum states whose decomposition exists in the aforementioned sense are referred to as *product states*, while qbits/qregisters tied together by the aforementioned phenomenon are referred to as *entangled states*. Entanglement is an efficient tool of quantum computing and communications, which facilitates the "science fiction concept of teleporting, communication over zero-capacity channels" and, more realistically, fast algorithms. However, commercial "quantum PCs" and "quantum phones" are absent from the shelves of electronics shops. Nonetheless, emerging quantum communications applications are already available on the market, for example, in the field of quantum cryptography, while a range of further applications are close to practical implementation.

Finally, it is worth mentioning that despite the fact that Einstein initiated the quest for the clarification of the quantum rules, he never accepted the concept of entanglement (he referred to it as a "*spooky action at a distance*") in his highly acclaimed thought experiment known as the Einstein, Podolsky, and Rosen (EPR) paradox published in 1935 [146]. Just to mention one of the "spooky actions at a distance," when observing an entangled qbit, its sheer observation instantaneously changes its entangled counterpart, regardless of its geographic position, which implies a propagation velocity higher than that of light.

B. Quantum-Assisted Communications

In wireless systems, there is always a tradeoff between reducing the transmit power and mitigating the resultant signal degradation imposed by the transmit-power reduction with the aid of sophisticated receiver algorithms, when considering the total energy consumption. This is because more sophisticated receivers dissipate more power. The associated relationship becomes even more complex in a multiuser networking context. Ideally, our design objective should be that of minimizing the *total* power consumption assigned to both transmission over the ether and to the SP electronics. More explicitly, it is neither economical nor "green" to invoke the most powerful available SP techniques owing to their high power consumption, unless the achievable *total* transmit power reduction or some other design constraints, such as a severely limited available frequency band, justifies this. This is because, in general, the bandwidth efficiency and power efficiency are inversely proportional to each other.

Quantum-assisted wireless communications exploits the extra computing power offered by quantum-mechanics-based architectures. This section summarizes some recent results in quantum computing and the corresponding application areas in wireless communications.

Grover published his quantum-domain database search algorithm in [147] and [148] to illustrate its benefits. This algorithm is capable of searching through *unsorted* databases by initiating parallel database queries and evaluating the answers in parallel. Notwithstanding its efficiency, Grover's solutions require several consecutive "query–evaluation" pairs, nonetheless, they only necessitate on the order of $\mathcal{O}(\sqrt{N})$ iterations to carry out the search compared to the classically required $\mathcal{O}(N)$ complexity, where N is the size of the search space. It was shown to be optimal in terms of the number of iterations [149]. As a further advance, Boyer *et al.* [150], [169] then enhanced the original algorithm by making it capable of finding M occurrences of the requested entry in the database and introduced upper bounds for the required number of operations, which was found to be on the order of $\mathcal{O}(\sqrt{N/M})$. Unfortunately, the results of Grover's algorithm are probabilistic in the sense that they provide the database index of the requested item with an error probability of $P_{\text{err}} \approx M/N$. Following a range of further improvements, such as, for example, the elimination of the probability of error without increasing the imposed computational complexity as well as tolerating the nonuniform distribution of the provided input database indices, for example, by another quantum algorithm, the most general form of quantum database search algorithms was then disseminated in [140]. Similar database search problems are also often encountered in wireless communications, for example, when finding the most suitable resource allocation, which results in the lowest level of cochannel interference across the entire network.

To elaborate a little further on the potential quantum-based communications techniques of the future, searching through unsorted databases may be viewed as being equivalent to finding certain points of a function $y = f(x)$, such as the minimum or maximum of a CF. Just to mention a few examples in wireless communications, we are typically

looking for the specific K-user bit vector, which maximizes the CF of a MUD, or of a multistream MIMO detector, etc. Unfortunately, classic MUD or MIMO-detector solutions suffer from a high computational complexity if the database is unsorted, or equivalently, if the related CF has numerous local minimum/maximum points.

For example, the ML MUD of a $K = 10$ user 64-QAM wireless system would have to evaluate the MMSE CF for all legitimate symbol combinations, namely 64^{10} times, which is clearly unrealistic. Furthermore, multiple CF optima may exist, when there are more transmit antennas in a MIMO system than the number of receiver antennas, because in this scenario, the channel matrix becomes a nonsquare, rank-deficient, and hence noninvertible matrix. Similar problems are also often encountered in resource-allocation techniques, when, for example, an MS has to search through the list of potential handover target BSs to find the one providing the best signal quality. In [151], the classic logarithmic search, which is known to be efficient for sorted databases, has been combined with quantum-based "existence testing" in order to answer the question as to whether the database does contain a specific entry at all. As alluded to above, MUDs or multistream MIMO detectors may also be viewed as the optimization of carefully chosen CFs.

The scope of the aforementioned K-user DS-CDMA MLS CF may be further extended, in order to handle an entire burst of symbols $b_k[i]$ for the K users. Naturally, in the absence of any channel-induced dispersion, i.e., ISI, there would be no benefit in considering several consecutive bits during the decision process, since they are independent of each other. However, in case of practical ISI-contaminated dispersive channels, this so-called *jointly optimum decision* would mitigate/eliminate both the MUI and ISI by estimating R symbols, rather than a single symbol, of all the K users jointly during a given DS-CDMA transmission burst. This results in a potentially excessive search space, which would be unrealistic to search through with the aid of conventional search/detection techniques. Hence, classic MUDs generate an estimate $\tilde{b}_k[i]$ for the K users on a symbol-by-symbol basis.

Having considered the basic philosophy of "quantumized" search/optimization techniques, let us now continue by stipulating the optimization CF, which potentially has a more grave influence on the final result than the choice of the specific optimization technique employed. We can use, for example, the classic zero forcing (ZF) and the minimum mean square error (MMSE) CF, as well as the more recently proposed direct minimum BER (MBER) CF, which were used in a MIMO multistream detection context in [11] and the MLS estimation criterion.

The first version of the aforementioned quantum-assisted multiuser detection (QMUD) method was published in [152] and improved in [140] and [153]. A range of other closely related approaches have been introduced during the period of 2000–2010. For example, Li *et al.* applied quantum neural networks in [154], while Gao *et al.* [155] introduced a quantum bee colony optimization (QBCO) technique for solving the aforementioned MUD problem.

C. Quantum-Based Communications

The rudiments of classic information-theoretic capacity were highlighted and relied upon in the earlier parts of this treatise, but its generalization to quantum information theory [142] is beyond the scope of this paper. Instead, we adopt a more practical approach and review a few quantum-communication-related aspects.

Suffice to say that the classic Shannonian entropy $H(p)$ has to be replaced by the so-called quantum entropy $S(\rho)$ of von Neumann [141], when we want to quantify the information content of a quantum source. Naturally, the $\mathcal{N}$ quantum channels may be regarded as an extension of the N classic channels, as detailed in [141], noting that some similarities to the complex baseband equivalent description widely used in wireless communication may be observed [156]. As an important application example, the error correction techniques of classic wireless communications have also been extended to quantum channels. More specifically, various block-coding methods were developed in [141], while pilot-symbol-based solutions have appeared in [157].

Let us now turn our attention to the realms of opportunities opened up by communications over quantum channels. Naturally, their capacity is one of the key aspects of their promise in future communications. Classically, the MI between the channel's input and output has to be maximized [158]. In case of quantum channels, the capacity had to be redefined, potentially leading to diverse scenarios to be considered. A natural distinction concerning the channel capacity definition is whether we restrict ourselves to classic inputs/outputs. In the former case of classic inputs/outputs, we encode the input symbols/states into quantum states, send them over the channel, and carry out a decision at the receiver side, effectively constructing a "classic–quantum–classic" processing chain. This is a natural approach, since humans can only process classic information. By contrast, if we do not restrict ourselves to classic inputs/outputs, we are capable of dealing with quantum channels within larger quantum systems. The most important question arising in this context is whether quantum channels are capable at all of increasing the achievable capacity, and if so, under what conditions.

The classic capacity of quantum channels has been quantified for decomposable product state inputs in the form of the so-called *unentangled classical capacity*, which is also often referred to as the Holevo–Schumacher–Westmoreland (HSW) capacity denoted by $C(\mathcal{N})$. In order to highlight the power behind the application of quantum channels, let us consider a rudimentary example. The classical binary symmetric channel (BSC), which either inverts or leaves an input bit with a probability of

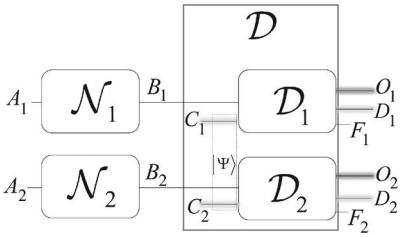

Fig. 20. ***Superactivation of zero-capacity quantum channels.***

$p = 1/2$ unchanged, has zero capacity quantified as $C(N) = 1 - H(p) = 0$. However, we may readily construct an appropriate classic single bit to single-qbit encoding at the transmitter and the corresponding detector at the receiver [159], so that all the classic bits transmitted over the channel will be received correctly with a unity probability, i.e., we have $C(\mathcal{N}) = 1$. As a stunning consequence, redundancy-free error correction is possible over noisy transmission media, at least for a specific subset of quantum channels. The rationale of this extraordinary statement may be traced back to the increased degree of freedom associated with the encoding and decoding processes introduced by the first postulate.

The science fiction saga continues. One of the hot research topics in this field is referred to as *superactivation* [160]. Naturally, in contrast to the previous striking example, there are also numerous quantum channels, which have zero capacity in the context of classic information transmission. Nonetheless, when considering two of these channels used in a parallel manner and, additionally applying the "entanglement-controlled" decoder architecture $\mathcal{D}$ of Fig. 20, the pair of quantum channels $\mathcal{N}_1$ and $\mathcal{N}_2$ succeed in delivering classic information over the $A_1 - O_1$ and $A_2 - O_2$ links. In other words, their capacities have been (super)activated, where A_1 and $A2$ are the channel inputs, while B_1 and B_2 are the corresponding channel outputs linked to the decoder. This superactivation may be achieved by coupling the two subdecoders $\mathcal{D}_1$ and $\mathcal{D}_2$ with the aid of the entangled state $|\Psi\rangle$ of inputs C_1 and C_2. The outputs O_1 and O_2 of the decoder provide the payload information, while D_i and F_i have an auxiliary role, since they guarantee that the operator describing the overall operation of the decoder remains unitary. Current research aims to complete the set of those channels which can be superactivated.

Concerning the *entanglement-assisted capacity* $C_E(\mathcal{N})$, when the qbits at the channel's input are conditioned to be entangled, a plethora of open questions are under discussion. Perhaps the most challenging one to answer is whether entanglement is capable of increasing the attainable capacity.

A promising, but rather specific, application of quantum channels is constituted by secret quantum key distribution techniques conceived for exchanging the classic encryption keys, which can be used for symmetric-key cryptography between distant locations. In order to indicate the importance of this area, information theoreticians have defined the *private capacity* $C_P(\mathcal{N})$ of quantum channels from a secure classic information transmission perspective [161].

If quantum information is fed into the quantum channel, the so-called *quantum capacity* $Q(\mathcal{N})$, which is also referred to as the Lloyd–Shor–Devetak (LSD) capacity [162], has to be considered, which is expected to be upper-bounded by the classic capacity of the same channel. In this context, the MUD problem also exists in quantum channels, as discussed in [163] and [164]. For detailed discussions on quantum information theory, refer to [142].

V. CONCLUSION

Many important aspects of contemporary wireless solutions have not even been touched upon owing to space limitations, such as the benefits of ultrawideband (UWB) systems [165] or cognitive radios (CR) [166], [167], just to mention a few of the essential elements of the wireless landscape.

Again, over the past three decades, a 1000-fold bit rate improvement was achieved, which facilitated the introduction of the powerful new wireless services featured in the stylized illustration of Fig. 2. These enticing, but bandwidth-hungry and power-thirsty, multimedia services "absorbed" the aforementioned bitrate improvements. Furthermore, the increased popularity and wealth-creation potential of conventional mobile phones, smarphones, and tablet computers resulted in the unprecedented penetration of wireless communications, as indicated in Fig. 1. As a result, the amount of teletraffic is expected to substantially increase during the next decade, which requires new frequency bands. As a result, the RF bands gradually migrated from 450 MHz, 900 MHz, 2 GHz, 5 GHz, 60 GHz, and beyond to the terahertz optical domain.

Regretfully, as the carrier frequency is increased, the pathloss tends to increase and the RF propagation properties gradually become reminiscent of those of visible light. Hence, the cell size has been reduced over the past decades from the original 35-km rural GSM cells to small urban picocells. Since plenty of unlicensed bandwidth is available in the optical frequency domain, cutting edge new research is required for achieving the same level of maturity in OW communications, as in RF engineering.

Additionally, radical advances are required in both quantum information theory to set out the theoretical performance limits, like Shannon did for classic communications, and in the quantum-domain counterparts of RF transceivers capable of approaching the quantum information theoretic predictions.

Again, this was not even touched upon in this treatise, nonetheless, we would like to close by alluding to flawless telepresence, which requires the extension of

the transceiver design principles provided in this treatise to compelling future services, with an ambience of joy and wonder. The recent advances in 3-D and holographic displays [168] facilitate immersive, flawless telepresence with the aid of the stereoscopic video toolbox of the H.264/MPEG4 codec, provided, of course, that a sufficiently high-speed, high-integrity wireless link is available.

The holographic video displays available on the market are set to revolutionize telecommunications, as the emergence of mobile communications has done two decades ago, leading to flawless telepresence. However, the error-resilient streaming of multiview and 3-D holographic video using OW and quantum-domain transceivers constitutes a further challenge. ■

NOMENCLATURE

3GPP	3rd Generation Partnership Project.
ADC	Analog-to-digital converter.
AF	Amplify-and-forward.
ALMMSE	Approximate linear minimum mean square error.
AMC	Adaptive modulation and coding.
AWGN	Additive white Gaussian noise.
BCJR	Bahl–Cocke–Jelinek–Raviv.
BER	Bit error ratio.
BLER	Block error ratio.
CIR	Channel impulse response.
CF	Cost function.
CC	Channel coding.
CE	Channel estimator.
CDMA	Code-division multiple access.
CLSM	Closed-loop spatial multiplexing.
CPICH	Common pilot channel.
CQI	Channel quality indicator.
CRC	Cyclic redundancy check.
CSI	Channel state information.
CSIR	Channel state information at the receiver.
CSIT	Channel state information at the transmitter.
CTC	Convolutional turbo code.
DCO-OFDM	Direct current optical-orthogonal frequency-division multiplexing.
DD	Direct detection.
DF	Decode-and-forward.
DFT	Discrete Fourier transform.
DL	Downlink.
D-TxAA	Double transmit antenna array.
FOV	Field of view.
FIFO	First-in–first-out.
FFT	Fast Fourier transform.
HARQ	Hybrid automated repeat request.
HSPA	High-speed packet access.
HSDPA	High-speed downlink packet access.
HS-PDSCH	High-speed physical downlink shared channel.
ICI	Intercarrier interference.
IFFT	Inverse fast Fourier transform.
IM	Intensity modulation.
IR	Infrared.
LAN	Local area network.
LDPC	Low-density parity check.
LED	Light-emitting diode.
LLR	Log-likelihood ratio.
LS	Least squares.
LTE	Long-term evolution.
LTE-A	Long-term evolution advanced.
LMMSE	Linear minimum mean square error.
LMMSE-MAP	Linear minimum mean square error maximum *a posteriori*.
LOS	Line-of-sight.
MAP	Maximum *a posteriori*.
MCRT	Monte Carlo ray tracing.
MI	Mutual information.
MIMO	Multiple-input–multiple-output.
MISO	Multiple-input–single-output.
ML	Maximum likelihood.
MSE	Mean square error.
MF-MIMO	Multifunctional MIMO.
NLOS	Non-line-of-sight.
OFDM	Orthogonal frequency-division multiplexing.
OFDMA	Orthogonal frequency-division multiple access.
OLSM	Open-loop spatial multiplexing.
OW	Optical wireless.
PAM	Pulse amplitude modulation.
PCCPCH	Primary common control physical channel.
PCI	Precoding control indicator.
PD	Photodetector.
PMI	Precoding matrix indicator.
PDP	Power delay profile.
QAM	Quadrature amplitude modulation.
RAID	Redundant array of inexpensive disks.
RI	Rank indicator.
RF	Radio frequency.
RMS	Root mean square.
RRC	Root raised cosine.
RS-CC	Reed–Solomon/convolutional code.
SC	Single carrier.
SCH	Synchronization channel.
SIMO	Single-input–multiple-output.
SINR	Signal-to-interference-and-noise ratio.
SIR	Signal-to-interference ratio.
SNR	Signal-to-noise ratio.
TBS	Transport block size.
TDMA	Time-division multiple access.
TIA	Transimpedance amplifier.
TxAA	Transmit antenna array.
TxD	Transmit diversity.

UE	User equipment.
UMTS	Universal Mobile Telecommunications System.
VLC	Visible light communication.
VLCC	Visible Light Communication Consortium.
WiFi	Wireless fidelity.
WiMAX	Worldwide interoperability for microwave access.
W-CDMA	Wideband code-division multiple access.
WLAN	Wireless local area network.

Acknowledgment

The authors would like to thank S. Caban and C. Mehlführer for their expert support of the measurements as well as S. Schwarz for providing LTE simulations and preparing Figs. 9–11 at the University of Technology, Vienna, Austria. They would also like to thank the current and past members of the optical wireless communications groups at Oxford University, Oxford, U.K., and The University of Edinburgh, Edinburgh, U.K., for their contributions to the work reported in this treatise, especially S. Dimitrov for providing the results on optical wireless networking. H. Haas would also like to acknowledge the support of the work on the optical wireless networking by Airbus Germany. L. Hanzo would like to thank his colleagues at the University of Southampton, U.K., in particular, J. Akhtman and R. Steels for the enlightenment gained from past and present collaborations.

REFERENCES

[1] L. Hanzo, M. El-Hajjar, and O. Alamri, "Near-capacity wireless transceivers and cooperative communications in the MIMO era: Evolution of standards, waveform design, and future perspectives," *Proc. IEEE*, vol. 99, no. 8, pp. 1343–1385, Aug. 2011.

[2] R. Steele and L. Hanzo, *Mobile Radio Communications: Second and Third Generation Cellular and WATM Systems*, 2nd ed. Chichester, U.K.: Wiley, 1999.

[3] L. Hanzo, L.-L. Yang, E.-L. Kuan, and K. Yen, *Single and Multi-Carrier DS-CDMA: Multi-User Detection, Space-Time Spreading, Synchronisation, Networking and Standards*. Chichester, U.K.: Wiley/IEEE Press, 2003.

[4] L. Hanzo, J. Blogh, and S. Ni, *3G, HSPA and FDD Versus TDD Networking: Smart Antennas and Adaptive Modulation*. New York: Wiley/IEEE Press, 2008.

[5] L. Hanzo, C. H. Wong, and M. S. Yee, Adaptive Wireless Transceivers: Turbo-Coded, Turbo-Equalized and Space-Time Coded TDMA, CDMA and OFDM Systems. Chichester, U.K.: Wiley/IEEE Press, 2002.

[6] L. Hanzo, M. Münster, B. J. Choi, and T. Keller, *OFDM and MC-CDMA for Broadband Multi-User Communications, WLANs and Broadcasting*. Chichester, U.K.: Wiley/IEEE Press, 2003.

[7] L. Hanzo, J. Akhtman, L. Wang, and M. Jiang, *MIMO-OFDM for LTE, WIFI and WIMAX: Coherent Versus non-Coherent and Cooperative Turbo-Transceivers*. Chichester, U.K.: Wiley/IEEE Press, 2010.

[8] International Telecommunication Union (ITU), *Measuring the Information Society*, 2011.

[9] S. Y. Yoon, "Introduction to WiBro Technology," Samsung Electronics Co., Ltd., Sep. 2004. [Online]. Available: http://www.itu.int/ITU-D/imt-2000/documents/Busan/Session3_Yoon.pdf

[10] C. Shannon, "Communication in the presence of noise," *Proc. IRE*, vol. 37, no. 1, pp. 10–22, Jan. 1949.

[11] S. Sugiura, S. Chen, and L. Hanzo, "MIMO-aided near-capacity turbo transceivers: Taxonomy and performance versus complexity," *IEEE Commun. Surveys Tuts.*, 2012, DOI: 10.1109/SURV.2011.032511.00136.

[12] G. J. Foschini, "Layered space-time architecture for wireless communication in a fading environment when using multiple antennas," *Bell Labs. Tech. J.*, vol. 1, no. 2, pp. 41–59, Autumn 1996.

[13] S. M. Alamouti, "A simple transmit diversity technique for wireless communications," *IEEE J. Sel. Areas Commun.*, vol. 16, no. 8, pp. 1451–1458, Oct. 1998.

[14] V. Tarokh, A. Naguib, N. Seshadri, and A. R. Calderbank, "Space-time codes for high data rate wireless communication: Performance criteria in the presence of channel estimation errors, mobility and multiple paths," *IEEE Trans. Commun.*, vol. 47, no. 2, pp. 199–207, Feb. 1999.

[15] L. Hanzo, T. H. Liew, B. L. Yeap, R. Y. S. Tee, and S. X. Ng, *Turbo Coding, Turbo Equalisation and Space Time Coding for Transmission Over Fading Channels*. Chichester, U.K.: Wiley/IEEE Press, 2011.

[16] G. Forney and D. Costello, "Channel coding: The road to channel capacity," *Proc. IEEE*, vol. 95, no. 6, pp. 1150–1177, Jun. 2007.

[17] T. Liew and L. Hanzo, "Space-time codes and concatenated channel codes for wireless communications," *Proc. IEEE*, vol. 90, no. 2, pp. 187–219, Feb. 2002.

[18] Nasruminallah and L. Hanzo, "Near-capacity h.264 multimedia communications using iterative joint source-channel decoding," *IEEE Commun. Surveys Tuts.*, 2012, DOI: 10.1109/SURV.2011.032211.00118.

[19] N. Bonello, S. Chen, and L. Hanzo, "Low-density parity-check codes and their rateless relatives," *IEEE Commun. Surveys Tuts.*, vol. 13, no. 1, pp. 3–26, First Quarter 2011.

[20] M. Butt, S. Ng, and L. Hanzo, "Self-concatenated code design and its application in power-efficient cooperative communications," *IEEE Commun. Surveys Tuts.*, 2012, DOI: 10.1109/SURV.2011.081511.00104.

[21] L. Wang and L. Hanzo, "Dispensing with channel estimation: Differentially modulated cooperative wireless communications," *IEEE Commun. Surveys Tuts.*, 2012, DOI: 10.1109/SURV.2011.081611.00138.

[22] E. Damosso, L. Stola, and G. Brussaard, "Characterisation of the 50–70 GHz band for space communications," *Eur. Space Agency J.*, vol. 7, no. 1, pp. 25–43, 1983.

[23] R. Ott and M. Thompson, "Atmospheric amplitude spectra in an absorption region," in *Proc. IEEE Antennas Propag. Soc. Symp.*, Amherst, MA, 1976, vol. 14, pp. 594–597.

[24] O. D. Lange, A. Dietrich, and D. C. Hogg, "An experiment on propagation of 60 GHz waves through rain," *Bell Syst. Tech. J.*, vol. 54, pp. 165–176, 1975.

[25] S. Chia, D. Greenwood, D. Rickard, C. Shephard, and R. Steele, "Propagation studies for a point-to-point 60 GHz micro-cellular system for urban environments," in *Proc. IEE Commun.*, Birmingham, U.K., 1986, pp. 28–32.

[26] T. Rappaport, J. Murdock, and F. Gutierrez, "State of the art in 60-GHz integrated circuits and systems for wireless communications," *Proc. IEEE*, vol. 99, no. 8, pp. 1390–1436, Aug. 2011.

[27] A. Ogasawara, "Energy issues confronting the information and communication sector," *NISTEP: Sci. Technol. Trends—Quarterly Rev.*, no. 21, Oct. 2006. [Online]. Available: www.nistep.go.jp/achiev/ftx/eng/stfc/stt021e/qr21pdf/STTqr2102.pdf

[28] EIA, "Average retail price of electricity to ultimate customers: Total by end-use sector," Energy Information Administration: Official Energy Statistics from the U.S. Government, May 2008. [Online]. Available: http://www.eia.doe.gov/cneaf/electricity/epm/table5_3.html

[29] A. Ghosh, D. R. Wolter, J. G. Andrews, and R. Chen, "Broadband wireless access with WiMax/802.16: Current performance benchmarks and future potential," *IEEE Commun. Mag.*, vol. 43, no. 2, pp. 129–136, Feb. 2005.

[30] H. Holma, A. Toskala, K. Ranta-aho, and J. Pirskanen, "High-speed packet access evolution in 3GPP release 7," *IEEE Commun. Mag.*, vol. 45, no. 12, pp. 29–35, Dec. 2007.

[31] E. Dahlman, S. Parkvall, J. Sköld, and P. Beming, *3G Evolution—HSPA and LTE for Mobile Broadband*, 1st ed. New York: Academic, 2007.

[32] S. Parkvall, E. Dahlman, A. Furuskar, Y. Jading, M. Olsson, S. Wanstedt, and K. Zangi, "LTE-advanced—Evolving LTE towards IMT-advanced," in *Proc. 68th IEEE Veh. Technol. Conf.*, Sep. 2008, DOI: 10.1109/VETECF.2008.313.

[33] TC LTE Group, *LTE Simulator Website*, 2009. [Online]. Available: http://www.nt.tuwien.ac.at/ltesimulator/

[34] P. Vandewalle, J. Kovacevic, and M. Vetterli, "Reproducible research in signal processing—What, Why, and How," *IEEE Signal Process. Mag.*, vol. 26, no. 3, pp. 37–47, May 2009.

[35] S. Caban, J. A. García-Naya, and M. Rupp, "Measuring the physical layer performance of wireless communication systems," *IEEE Instrum. Meas. Mag.*, vol. 14, no. 5, pp. 8–17, Oct. 2011.

[36] G. J. Foschini and M. J. Gans, "On limits of wireless communications in a fading environment when using multiple antennas," *Wireless Pers. Commun.*, vol. 6, no. 3, pp. 311–335, Mar. 1998.

[37] I. E. Telatar, "Capacity of multi-antenna Gaussian channels," *Eur. Trans. Telecommun.*, vol. 10, no. 6, pp. 585–595, Oct. 1998.

[38] L. Hanzo, O. Alamri, M. El-Hajjar, and N. Wu, *Near-Capacity Multi-Functional MIMO Systems: Sphere-Packing, Iterative Detection and Cooperation*. New York: IEEE Press/John Wiley, 2009.

[39] S. Verdu, "Spectral efficiency in the wideband regime," *IEEE Trans. Inf. Theory*, vol. 48, no. 6, pp. 1319–1343, Jun. 2002.

[40] G. Durisi, U. G. Schuster, H. Bölcskei, and S. Shamai (Shitz), "Noncoherent capacity of underspread fading channels," *IEEE Trans. Inf. Theory*, vol. 56, no. 1, pp. 367–395, Jan. 2010.

[41] J. Andrews, S. Shakkottai, R. Heath, N. Jindal, M. Haenggi, R. Berry, D. Guo, M. Neely, S. Weber, S. Jafar, and A. Yener, "Rethinking information theory for mobile ad hoc networks," *IEEE Commun. Mag.*, vol. 46, no. 12, pp. 94–101, Dec. 2008.

[42] A. Tulino, A. Lozano, and S. Verdu, "MIMO capacity with channel state information at the transmitter," in *Proc. Int. Symp. Spread Spectrum Tech. Appl.*, Sydney, Australia, Aug. 2004, pp. 22–26.

[43] C. Mehlführer, S. Caban, and M. Rupp, "Measurement-based performance evaluation of MIMO HSDPA," *IEEE Trans. Veh. Technol.*, vol. 59, no. 9, pp. 4354–4367, Nov. 2010.

[44] C. Mehlführer, S. Caban, and M. Rupp, "Cellular system physical layer throughput: How far off are we from the Shannon bound?" *IEEE Wireless Commun. Mag.*, vol. 18, no. 6, pp. 54–63, Dec. 2011.

[45] S. Caban, C. Mehlführer, M. Rupp, and M. Wrulich, *Evaluation of HSDPA to LTE: From Testbed Measurements to System Level Performance*. New York: Wiley-Blackwell, 2012.

[46] L. Hentilä, P. Kyösti, M. Käske, M. Narandzic, and M. Alatossava, *MATLAB Implementation of the WINNER Phase II Channel Model ver. 1.1*, Dec. 2007. [Online]. Available: http://www.ist-winner.org/phase_2_model.html

[47] C. Mehlführer, S. Caban, and M. Rupp, "Experimental evaluation of adaptive modulation and coding in MIMO WiMAX with limited feedback," *EURASIP J. Adv. Signal Process.*, vol. 2008, *Special Issue on MIMO Systems With Limited Feedback*, Article ID 837102, 2008. [Online]. Available: http://publik.tuwien.ac.at/files/pub-et_13762.pdf

[48] M. Rupp, C. Mehlführer, and S. Caban, "On achieving the Shannon bound in cellular systems," in *Proc. 20th Int. Conf. Radioelektronika*, Brno, Czech Republik, Apr. 2010. [Online]. Available: http://publik.tuwien.ac.at/files/PubDat_185403.pdf

[49] S. Caban, C. Mehlführer, G. Lechner, and M. Rupp, "Testbedding MIMO HSDPA and WiMAX," in *Proc. 70th IEEE Veh. Technol. Conf.*, Anchorage, Sep. 2009, DOI: 10.1109/VETECF.2009.5378995. [Online]. Available: http://publik.tuwien.ac.at/files/PubDat_176574.pdf

[50] B. Efron and D. V. Hinkley, *An Introduction to the Bootstrap*, 1st ed. London, U.K.: Chapman & Hall/CRC Press, 1994.

[51] S. Schwarz, M. Simko, and M. Rupp, "On performance bounds for MIMO OFDM based wireless communication systems," in *Proc. 12th IEEE Int. Workshop Signal Process. Adv. Wireless Commun.*, Jun. 2011, pp. 311–315.

[52] S. Schwarz and M. Rupp, "Throughput maximizing feedback for MIMO OFDM based wireless communication systems," in *Proc. 12th IEEE Int. Workshop Signal Process. Adv. Wireless Commun.*, Jun. 2011, pp. 316–320.

[53] A. Paulraj, R. Nabar, and D. Gore, *Introduction to Space-Time Wireless Communications*, 1st ed. Cambridge, U.K.: Cambridge Univ. Press, 2003.

[54] A. F. Molisch, *Wireless Communications*, 1st ed. New York: Wiley, 2005.

[55] L. M. Correia, Ed., *Wireless Flexible Personalised Communications*. New York: Wiley, 2001.

[56] J. P. Kermoal, L. Schumacher, K. I. Pedersen, P. E. Mogensen, and F. Frederiksen, "A stochastic MIMO radio channel model with experimental validation," *IEEE J. Sel. Areas Commun.*, vol. 20, no. 6, pp. 1211–1226, Aug. 2002.

[57] H. Hofstetter and G. Steinböck, "A geometric based stochastic channel model for MIMO systems," in *Proc. ITG Workshop Smart Antennas*, Munich, Germany, Mar. 2004, pp. 194–199.

[58] 3GPP, *Technical Specification Group Radio Access Network; Spatial Channel Model for Multiple Input Multiple Output (MIMO) Simulations (release 8)*, 3GPP TS 25.996 v8.0.0, Dec. 2008. [Online]. Available: http://www.ist-winner.org/3gpp_scm.html

[59] M. Rupp, J. A. García-Naya, C. Mehlführer, S. Caban, and L. Castedo, "On mutual information and capacity in frequency selective wireless channels," in *Proc. IEEE Int. Conf. Commun.*, Cape Town, South Africa, May 2010, DOI: 10.1109/ICC.2010.5501942. [Online]. Available: http://publik.tuwien.ac.at/files/PubDat_184660.pdf

[60] X.-Y. Hu, E. Eleftheriou, and D. Arnold, "Regular and irregular progressive edge-growth tanner graphs," *IEEE Trans. Inf. Theory*, vol. 51, no. 1, pp. 386–398, Jan. 2005.

[61] D. J. MacKay, "Good error-correcting codes based on very sparse matrices," *IEEE Trans. Inf. Theory*, vol. 45, no. 2, pp. 399–431, Mar. 1999.

[62] C. Mehlführer, S. Caban, and M. Rupp, "An accurate and low complex channel estimator for OFDM WiMAX," in *Proc. 3rd Int. Symp. Commun. Control Signal Process.*, St. Julians, Malta, Mar. 2008, pp. 922–926. [Online]. Available: http://publik.tuwien.ac.at/files/pub-et_13650.pdf

[63] M. Simko, S. Pendl, S. Schwarz, Q. Wang, J. C. Ikuno, and M. Rupp, "Optimal pilot symbol power allocation in LTE," in *Proc. IEEE 74th Veh. Technol. Conf.*, Sep. 2011, DOI: 10.1109/VETECF.2011.6092929.

[64] M. Simko and M. Rupp, "Optimal pilot symbol power allocation in multi-cell scenarios in LTE," in *Proc. 45th Asilomar Conf. Signal Syst. Comput.*, Pacific Grove, CA, Nov. 2011. [Online]. Available: http://publik.tuwien.ac.at/files/PubDat_200461.pdf

[65] B. M. Hochwald, "Cayley differential unitary space-time codes," *IEEE Trans. Inf. Theory*, vol. 48, no. 6, pp. 1485–1503, Jun. 2002.

[66] J. G. Proakis, Ed., *Digital Communications*, 3rd ed. New York: McGraw-Hill, 1995.

[67] F. R. Gfeller and U. Bapst, "Wireless in-house data communication via diffuse infrared radiation," *Proc. IEEE*, vol. 67, no. 11, pp. 1474–1486, Nov. 1979.

[68] H. Elgala, R. Mesleh, and H. Haas, "Indoor optical wireless communication: Potential and state-of-the-art," *IEEE Commun. Mag.*, vol. 49, no. 9, pp. 56–62, Sep. 2011.

[69] J. D. Barry, *Wireless Infrared Communications*. Norwell, MA: Kluwer, 1994.

[70] *Visible Light Communications Consortium*. [Online]. Available: www.vlcc.net

[71] *CP-1221 Japanese Visible Light Communications System*, Japan Electronics Industry Technology Association, 2007.

[72] *CP-1222 Japanese Visible Light ID System*, Japan Electronics Industry Technology Association, 2007.

[73] *IEEE Standard for Local and Metropolitan Area Networks—Part 15.7: Short-Range Wireless Optical Communication Using Visible Light*, IEEE, 2011.

[74] *IEC 60825-1. Safety of Laser Products Part 1*, International Electrotechnical Commission, British Standards Institution, 2007.

[75] P. L. Eardley, D. R. Wisely, D. Wood, and P. McKee, "Holograms for optical wireless LANs," *Inst. Electr. Eng. Proc.—Optoelectron.*, vol. 143, no. 6, pp. 365–369, 1996.

[76] A. C. Boucouvalas, "Indoor ambient light noise and its effect on wireless optical links," *Inst. Electr. Eng. Proc.—Optoelectron.*, vol. 143, no. 6, pp. 334–338, 1996.

[77] R. Winston, W. T. Welford, J. C. Minano, and P. Benitez, *Nonimaging Optics*. Amsterdam, The Netherlands: Elsevier, 2005.

[78] D. C. O'Brien, G. E. Faulkner, E. B. Zyambo, K. Jim, D. J. Edwards, P. Stavrinou, G. Parry, J. Bellon, M. J. Sibley, V. A. Lalithambika, V. M. Joyner, R. J. Samsudin, D. M. Holburn, and R. J. Mears, "Integrated transceivers for optical wireless communications," *IEEE J. Sel. Topics Quantum Electron.*, vol. 11, no. 1, pp. 173–183, Jan./Feb. 2005.

[79] V. Jungnickel, V. Pohl, S. Nonnig, and C. von Helmolt, "A physical model of the wireless infrared communication channel," *IEEE J. Sel. Areas Commun.*, vol. 20, no. 3, pp. 631–640, Apr. 2002.

[80] J. M. Kahn, W. J. Krause, and J. B. Carruthers, "Experimental characterization of non-directed indoor infrared channels," *IEEE Trans. Commun.*, vol. 43, no. 2–4, pp. 1613–1623, Feb./Mar./Apr. 1995.

[81] J. R. Barry and J. M. Kahn, "Link design for nondirected wireless infrared communications," *Appl. Opt.*, vol. 34, no. 19, pp. 3764–3776, 1995.

[82] J. Grubor, S. Randel, K. D. Langer, and J. W. Walewski, "Broadband information broadcasting using led-based interior lighting," *J. Lightw. Technol.*, vol. 26, no. 24, pp. 3883–3892, Dec. 15, 2008.

[83] H. Le-Minh, D. O'Brien, G. Faulkner, M. Wolf, L. Grobe, J. Lui, and O. Bouchet,

"A 1.25 Gbit/s Indoor optical wireless demonstrator," *IEEE Photon.Technol. Lett.*, vol. 22, no. 21, pp. 1598–1600, Nov. 1, 2010.

[84] D. O'Brien, R. Turnbull, H. Le Minh, G. Faulkner, M. Wolf, L. Grobe, J. Li, O. Bouchet, and E. Gueutier, "A 280 Mbit/s infrared optical wireless communications system," in *Proc. Free-Space Atmos. Laser Commun. XI*, San Diego, CA, 2011, vol. 8162, p. 81620K-6.

[85] A. J. Lowery and J. Armstrong, "10 Gbit/s multimode fiber link using power-efficient orthogonal-frequency-division multiplexing," *Opt. Exp.*, vol. 13, no. 25, pp. 10 003–10 009, 2005.

[86] J. Vucic, C. Kottke, S. Nerreter, K. D. Langer, and J. W. Walewski, "513 Mbit/s visible light communications link based on DMT-modulation of a white LED," *J. Lightw. Technol.*, vol. 28, no. 24, pp. 3512–3518, Dec. 15, 2010.

[87] J. Armstrong and A. Lowery, "Power efficient optical OFDM," *Electron. Lett.*, vol. 42, no. 6, pp. 370–372, 2006.

[88] R. Mesleh, H. Elgala, and H. Haas, "On the performance of different OFDM based optical wireless communication systems," *J. Opt. Commun. Netw.*, vol. 3, no. 8, pp. 620–628, 2011.

[89] S. Dimitrov and H. Haas, "On the clipping noise in an ACO-OFDM optical wireless communication system," in *Proc. IEEE Global Telecommun. Conf.*, 2010, DOI: 10.1109/GLOCOM.2010.5684301.

[90] D. Wisely and I. Neild, "A 100 Mbit/s tracked optical wireless telepoint," in *Proc. 8th Int. Symp. Pers. Indoor Mobile Radio Commun.*, 1997, vol. 3, pp. 964–968.

[91] J. B. Carruthers and J. M. Kahn, "Angle diversity for nondirected wireless infrared communication," *IEEE Trans. Commun.*, vol. 48, no. 6, pp. 960–969, Jun. 2000.

[92] G. Yun and M. Kavehrad, "Spot-diffusing and fly-eye receivers for indoor infrared wireless communications," in *Proc. IEEE Int. Conf. Sel. Topics Wireless Commun.*, 1992, pp. 262–265.

[93] P. Djahani and J. M. Kahn, "Analysis of infrared wireless links employing multibeam transmitters and imaging diversity receivers," *IEEE Trans. Commun.*, vol. 48, no. 12, pp. 2077–2088, Dec. 2000.

[94] F. Parand, G. E. Faulkner, and D. C. O'Brien, "Cellular tracked optical wireless demonstration link," *Inst. Electr. Eng. Proc.—Optoelectron.*, vol. 150, no. 5, pp. 490–496, 2003.

[95] S. Jivkova, B. A. Hristov, and M. Kavehrad, "Power-efficient multispot-diffuse multiple-input-multiple-output approach to broad-band optical wireless communications," *IEEE Trans. Veh. Technol.*, vol. 53, no. 3, pp. 882–889, May 2004.

[96] F. E. Alsaadi and J. M. H. Elmirghani, "Mobile multigigabit indoor optical wireless systems employing multibeam power adaptation and imaging diversity receivers," *J. Opt. Commun. Netw.*, vol. 3, no. 1, pp. 27–39, 2011.

[97] S. Hranilovic and F. Kschischang, "A pixelated MIMO wireless optical communication system," *IEEE J. Sel. Topics Quantum Electron.*, vol. 12, no. 4, pp. 859–874, Jul.-Aug. 2006.

[98] L. B. Zeng, D. C. O'Brien, H. Le Minh, G. E. Faulkner, K. Lee, D. Jung, Y. Oh, and E. T. Won, "High data rate multiple input multiple output (MIMO) optical wireless communications using white LED lighting," *IEEE J. Sel. Areas Commun.*, vol. 27, no. 9, pp. 1654–1662, Dec. 2009.

[99] R. Mesleh, H. Elgala, and H. Haas, "Optical spatial modulation," *IEEE/OSA J. Opt. Commun. Netw.*, vol. 3, no. 3, pp. 234–244, Mar. 2011.

[100] K. Dambul, D. O'Brien, and G. Faulkner, "Indoor optical wireless MIMO system with an imaging receiver," *IEEE Photon. Technol. Lett.*, vol. 23, no. 2, pp. 97–99, Jan. 15, 2011.

[101] L. Hanzo, M. El-Hajjar, and O. Alamri, "Near-capacity wireless transceivers and cooperative communications in the MIMO era: Evolution of standards, waveform design, and future perspectives," *Proc. IEEE*, vol. 99, no. 8, pp. 1343–1385, Aug. 2011.

[102] S. Sugiura, S. Chen, and L. Hanzo, "Mimo-aided near-capacity turbo transceivers: Taxonomy and performance versus complexity," *IEEE Commun. Surveys Tuts.*, 2011, DOI: 10.1109/SURV.2011.032511.00136.

[103] S. Sugiura, S. Chen, and L. Hanzo, "A universal space-time architecture for multiple-antenna aided systems," *IEEE Commun. Surveys Tuts.*, 2011, DOI: 10.1109/SURV.2011.041911.00105.

[104] H. Le Minh, D. O'Brien, G. Faulkner, L. B. Zeng, K. Lee, D. Jung, Y. Oh, and E. T. Won, "100-Mb/s NRZ visible light communications using a postequalized white LED," *IEEE Photon. Technol. Lett.*, vol. 21, no. 15, pp. 1063–1065, Aug. 1, 2009.

[105] K. Wang, A. Nirmalathas, C. Lim, and E. Skafidas, "4× 12.5 Gb/s WDM optical wireless communication system for indoor applications," *J. Lightw. Technol.*, vol. 29, no. 13, pp. 1988–1996, Jul. 1, 2011.

[106] A. Khanifar and R. J. Green, "Photoparametric amplifiers for subcarrier-multiplexed communication systems," *Inst. Electr. Eng. Proc.—Optoelectron.*, vol. 146, no. 5, pp. 223–229, 1999.

[107] G. Gilbreath and W. Rabinovich, "Research in free-space optical data transfer at the U.S. Naval Research Laboratory," *Proc. SPIE—Int. Soc. Opt. Eng.*, vol. 5160, no. 1, pp. 225–233, 2004.

[108] Z. Huanlin, A. Seetharaman, P. Johnson, L. Guipeng-Luo, and H. Le, "High-gain low-noise mid-infrared quantum cascade optical preamplifier for receiver," *IEEE Photon. Technol. Lett.*, vol. 17, no. 1, pp. 13–15, Jan. 2005.

[109] D. C. O'Brien and M. Katz, "Invited. optical wireless communications within fourth-generation wireless systems," *J. Opt. Netw.*, vol. 4, no. 6, pp. 312–322, 2005.

[110] J. Hou and D. O'Brien, "Vertical handover-decision-making algorithm using fuzzy logic for the integrated Radio-and-OW system," *IEEE Trans. Wireless Commun.*, vol. 5, no. 1, pp. 176–185, Jan. 2006.

[111] L. C. Andrews, R. L. Phillips, and C. Y. Hopen, *Laser Beam Scintillation With Applications*. Bellingham, WA: SPIE, 2001.

[112] I. B. Djordjevic, "Adaptive modulation and coding for free-space optical channels," *J. Opt. Commun. Netw.*, vol. 2, no. 5, pp. 221–229, May 2010.

[113] E. Lee and V. Chan, "Diversity coherent and incoherent receivers for free-space optical communication in the presence and absence of interference," *IEEE/OSA J. Opt. Commun. Netw.*, vol. 1, no. 5, pp. 463–483, Oct. 2009.

[114] S. Aghajanzadeh and M. Uysal, "Diversity–multiplexing trade-off in coherent free-space optical systems with multiple receivers," *IEEE/OSA J. Opt. Commun. Netw.*, vol. 2, no. 12, pp. 1087–1094, Dec. 2010.

[115] G. K. Karagiannidis, T. A. Tsiftsis, and H. G. Sandalidis, "Outage probability of relayed free space optical communication systems," *Electron. Lett.*, vol. 42, no. 17, pp. 994–995, Aug. 2006.

[116] M. Safari and M. Uysal, "Relay-assisted free-space optical communication," *IEEE Trans. Wireless Commun.*, vol. 7, no. 12, pp. 5441–5449, Dec. 2008.

[117] C. Datsikas, K. Peppas, N. Sagias, and G. Tombras, "Serial free-space optical relaying communications over gamma-gamma atmospheric turbulence channels," *IEEE/OSA J. Opt. Commun. Netw.*, vol. 2, no. 8, pp. 576–586, Aug. 2010.

[118] M. Karimi and M. Nasiri-Kenari, "Outage analysis of relay-assisted free-space optical communications," *IET Commun.*, vol. 4, no. 12, pp. 1423–1432, Aug. 2010.

[119] R. C. Menendez and J. W. Gannet, "Efficient, fault-tolerant all-optical multicast networks via network coding," in *Proc. Opt. Fiber Commun./Nat. Fiber Opt. Eng. Conf.*, San Diego, CA, Feb. 2008, DOI: 10.1109/OFC.2008.4528116.

[120] K. Minkyu, M. Medard, and U. M. OReilly, "Network coding and its implications on optical networking," in *Proc. Opt. Fiber Commun./Nat. Fiber Opt. Eng. Conf.*, San Diego, CA, Feb. 2009.

[121] E. D. Manley, J. S. Deogun, L. Xu, and D. R. Alexander, "All-optical network coding," *IEEE/OSA J. Opt. Commun. Netw.*, vol. 2, no. 4, pp. 175–191, Apr. 2010.

[122] A. E. Kamal, "1+n network protection for mesh networks: Network coding-based protection using p-cycles," *IEEE/ACM Trans. Netw.*, vol. 18, no. 18, pp. 67–80, Feb. 2010.

[123] O. Shalvi, "Multiple source cooperation diversity," *IEEE Commun. Lett.*, vol. 8, no. 12, pp. 712–714, Dec. 2004.

[124] R. Zhang and L. Hanzo, "A unified treatment of superposition coding aided communications: Theory and practice," *IEEE Commun. Surveys Tuts.*, vol. 13, no. 3, pp. 503–520, Third Quarter 2011.

[125] R. Zhang and L. Hanzo, "Coding schemes for energy efficient multi-source cooperation aided uplink transmission," *IEEE Signal Proces. Lett.*, vol. 16, no. 5, pp. 438–441, May 2009.

[126] A. Farid and S. Hranilovic, "Channel capacity and non-uniform signalling for free-space optical intensity channels," *IEEE J. Sel. Areas Commun.*, vol. 27, no. 9, pp. 1553–1563, Dec. 2009.

[127] J. Anguita, M. Neifeld, B. Hildner, and B. Vasic, "Rateless coding on experimental temporally correlated FSO channels," *J. Lightw. Technol.*, vol. 28, no. 7, pp. 990–1002, Apr. 1, 2010.

[128] I. Djordjevic, B. Vasic, and M. Neifeld, "Multilevel coding in free-space optical MIMO transmission with Q-ary PPM over the atmospheric turbulence channel," *IEEE Photon. Technol. Lett.*, vol. 18, no. 14, pp. 1491–1493, Jul. 2006.

[129] I. Djordjevic, "Coded-orthogonal frequency division multiplexing in hybrid optical networks," *IET Optoelectron.*, vol. 4, no. 1, pp. 17–28, 2010.

[130] O. Bouchet, P. Porcon, J. W. Walewski, S. Nerreter, K. D. Langer, L. Fernandez, J. Vucic, T. Kamalakis, G. Ntogari, I. Neoskosmidis, and E. Gueutier, "Wireless optical network for a home network," *Free-Space Laser Commun. X*, vol. 7814, pp. 781406–781406-9, 2010.

[131] B. Ghimire and H. Haas, "Resource allocation in optical wireless networks," *Proc. IEEE Int. Symp. Pers. Indoor Mobile Radio Commun.*, Toronto, ON, Canada, 2011, pp. 1061–1065.

[132] S. Dimitrov, R. Mesleh, H. Haas, M. Cappitelli, M. Olbert, and E. Bassow, "On the SIR of a cellular infrared optical wireless system for an aircraft," *IEEE J. Sel. Areas Commun.*, vol. 27, no. 9, pp. 1623–1638, Dec. 2009.

[133] Y. Tanaka, T. Komine, S. Haruyama, and M. Nakagawa, "Indoor visible communication utilizing plural white LEDs as lighting," in *Proc. 12th IEEE Int. Symp. Pers. Indoor Mobile Radio Commun.*, San Diego, CA, Sep. 30–Oct. 3, 2001, vol. 2, pp. 81–85.

[134] M. Z. Afgani, H. Haas, H. Elgala, and D. Knipp, "Visible light communication using OFDM," in *Proc. IEEE 2nd Int. Conf. Testbeds Res. Infrastructures Develop. Netw. Communities*, Barcelona, Spain, Mar. 1–3, 2006, pp. 129–134.

[135] J. Armstrong and B. J. C. Schmidt, "Comparison of asymmetrically clipped optical OFDM and DC-biased optical OFDM in AWGN," *IEEE Commun. Lett.*, vol. 12, no. 5, pp. 343–345, May 2008.

[136] 3GPP, *Evolved Universal Terrestrial Radio Access (E-UTRA); Radio Frequency (RF) System Scenarios*, 3GPP TR 36.942 V 8.2.0 (2009-05), May 2009. [Online]. Available: www.3gpp.org/ftp/Specs/

[137] J. Akhtman and L. Hanzo, "Heterogeneous networking: An enabling paradigm for ubiquitous wireless communications," *Proc. IEEE*, vol. 98, no. 2, pp. 135–138, Feb. 2010.

[138] R. D. Feynmann, *QED: The Strange Theory of Light and Matter*. Princeton, NJ: Princeton Univ. Press, 1985.

[139] R. Shankar, *Principles of Quantum Mechanics*. New York: Springer-Verlag, 1994.

[140] S. Imre and F. Balazs, *Quantum Computing and Communications—An Engineering Approach*. New York: Wiley, 2005.

[141] M. A. Nielsen and I. L. Chuang, *Quantum Computation and Quantum Information*. Cambridge, U.K.: Cambridge Univ. Press, 2000.

[142] D. Petz, *Quantum Information Theory and Quantum Statistics*. New York: Springer-Verlag, 2011.

[143] P. A. Dirac, *The Principles of Quantum Mechanics*. Oxford, U.K.: Oxford Univ. Press, 1982.

[144] J. S. Bell, "On the problem of hidden variables in quantum mechanics," *Rev. Modern Phys.*, vol. 38, pp. 447–452, 1964.

[145] J. F. Clauser, M. A. Horne, A. Shimony, and R. A. Holt, "Proposed experiment to test local hidden-variable theories," *Phys. Rev. Lett.*, vol. 23, pp. 880–884, 1969.

[146] A. Einstein, B. Podolsky, and N. Rosen, "Can quantum-mechanical description of physical reality be considered complete?" *Phys. Rev.*, vol. 47, pp. 777–780, 1935.

[147] L. Grover, "A fast quantum mechanical algorithm for database search," in *Proc. 28th Annu. ACM Symp. Theory Comput.*, May 1996, pp. 212–219. [Online]. Available: quant-ph/9605043

[148] L. K. Grover, "Quantum mechanics helps in searching for a needle in a haystack," *Phys. Rev. Lett.*, vol. 79, no. 2, pp. 325–328, Jul. 1997. [Online]. Available: quant-ph/9706033

[149] C. Zalka, "Grover's quantum searching algorithm is optimal," *Phys. Rev. A*, vol. 60, pp. 2746–2751, 1999.

[150] M. Boyer, G. Brassard, P. Hoyer, and A. Tapp, "Tight bounds on quantum searching," in *Proc. 4th Workshop Phys. Comput.*, 1996, vol. 46, no. 4–5, pp. 36–43.

[151] S. Imre, "Quantum existence testing and its application for finding extreme values in unsorted databases," *IEEE Trans. Comput.*, vol. 56, no. 5, pp. 706–710, May 2007.

[152] S. Imre and F. Balazs, "Non-coherent multi-user detection based on quantum search," in *Proc. IEEE Int. Conf. Commun.*, New York, Apr. 28–May 2, 2002, pp. 283–287.

[153] S. M. Zhao, J. Yao, and B. Y. Zheng, "Multiuser detection based on Grover's algorithm," in *Proc. IEEE Int. Symp. Circuits Syst.*, May 21–24, 2006, DOI: 10.1109/ISCAS.2006.1693688.

[154] F. Li, S. M. Zhao, and B. Y. Zheng, "Quantum neural network for CDMA multi-user detection," *Lecture Notes in Computer Science*, vol. 3498. Berlin, Germany: Springer-Verlag, 2005.

[155] H. Y. Gao, Y. Q. Liu, and M. Diao, "Robust multi-user detection based on quantum bee colony optimisation," *Int. J. Innovative Comput. Appl.*, vol. 3, no. 3, pp. 160–168, 2011.

[156] D. Petz, *Quantum Information Theory and Quantum Statistics*. Heidelberg, Germany: Springer-Verlag, 2008.

[157] L. Bacsardi, L. Gyongyosi, and S. Imre, "Redundancy-free quantum coding methods in satellite communications," Int. Astronaut. Congr., Cape Town, South Africa, Oct. 3–7, 2011.

[158] C. E. Shannon, "Communication theory of secrecy systems," *Bell Syst. Tech. J.*, vol. 28, pp. 656–715, 1949.

[159] L. Bacsardi, M. Berces, and S. Imre, "Redundancy-free quantum theory based error correction method in long distance aerial communication," *9th Int. Astronaut. Congr.*, Glasgow, U.K., Sep. 29–Oct. 3, 2011.

[160] G. Smith and J. Yard, "Quantum communication with zero-capacity channels," *Science*, vol. 321, pp. 1812–1815, 2008.

[161] I. Devetak, "The private classical capacity and quantum capacity of a quantum channel," *IEEE Trans. Inf. Theory*, vol. 51, no. 1, pp. 44–55, Jan. 2003.

[162] S. Lloyd, "Capacity of the noisy quantum channel," *Phys. Rev. A*, vol. 55, pp. 1613–1622, 1997.

[163] J. I. Concha and H. V. Poor, "Multi-access quantum channels," *IEEE Trans. Inf. Theory*, vol. 50, no. 5, pp. 725–747, May 2004.

[164] S. M. Zhao, F. Gao, X. L. Dong, and B. Y. Zheng, "Quantum multi-user detection scheme with discrete coherent states approximation," in *Proc. IEEE 10th Int. Conf. Signal Process.*, Oct. 24–28, 2010, pp. 1569–1572.

[165] A. Molisch, "Ultra-wide-band propagation channels," *Proc. IEEE*, vol. 97, no. 2, pp. 353–371, Feb. 2009.

[166] A. Molisch, L. Greenstein, and M. Shafi, "Propagation issues for cognitive radio," *Proc. IEEE*, vol. 97, no. 5, pp. 787–804, May 2009.

[167] A. Goldsmith, S. Jafar, I. Maric, and S. Srinivasa, "Breaking spectrum gridlock with cognitive radios: An information theoretic perspective," *Proc. IEEE*, vol. 97, no. 5, pp. 894–914, May 2009.

[168] A. M. Tekalp, A. Smolic, A. Vetro, and L. Onural, Eds., *Proc. IEEE*, vol. 99, *Special Issue on 3D Media and Displays*, no. 4, Apr. 2011.

[169] M. Boyer, G. Brassard, P. Hoyer, and A. Tapp, "Tight bounds on quantum searching," *Fortschritte der Physik*, vol. 46, no. 4–5, pp. 493–505, 1998.

ABOUT THE AUTHORS

Lajos Hanzo (Fellow, IEEE) received the M.S. degree, the Ph.D. degree, and the Honorary Doctorate "Doctor Honaris Causa" degree, all from the Technical University of Budapest, Budapest, Hungary, in 1976, 1983, and 2009, respectively.

During his 35-year career in telecommunications, he has held various research and academic posts in Hungary, Germany, and the United Kingdom. Since 1986, he has been with the School of Electronics and Computer Science, University of Southampton, Southampton, U.K., where he holds the Chair in Telecommunications. Since 2009, he has been a Chaired Professor with Tsinghua University, Beijing, China. He has successfully supervised more than 70 Ph.D. students. He is currently directing an academic research team, working on a range of research projects in the field of wireless multimedia communications sponsored by industry, the U.K. Engineering and Physical Sciences Research Council, the European IST Program, and the U.K. Mobile Virtual Centre of Excellence. He is an enthusiastic supporter of industrial and academic liaison, and he offers a range of industrial courses.

Dr. Hanzo is a Governor of the IEEE Vehicular Technology Society and a Fellow of the Royal Academy of Engineering, Institution of Engineering and Technology, and the European Association for Signal Processing. Since 2008, he has been the Editor-in-Chief of the IEEE Press. He coauthored 20 John Wiley/IEEE Press books on mobile radio communications totaling more than 10 000 pages, published more than 1200 research entries on IEEE Xplore, acted as both Technical Program Chair and General Chair of IEEE conferences, and presented keynote lectures. He has received a number of distinctions.

Harald Haas (Member, IEEE) received the Ph.D. degree in wireless communications from the University of Edinburgh, Edinburgh, U.K., in 2001.

He holds the Chair of Mobile Communications in the Institute for Digital Communications (IDCOM), University of Edinburgh and he currently is the CTO of a university spinoff company VLC Ltd. His main research interests are in interference coordination in wireless networks, spatial modulation, and optical wireless communication. He holds more than 15 patents. He has published more than 50 journal papers including a *Science* article and more than 150 peer-reviewed conference papers. Nine of his papers are invited papers. He has coauthored a book entitled *Next Generation Mobile Access Technologies: Implementing TDD* (Cambridge, U.K.: Cambridge Univ. Press, 2008). Since 2007, he has been a Regular High Level Visiting Scientist supported by the Chinese "111 program" at Beijing University of Posts and Telecommunications (BUPT), Beijing, China.

Prof. Haas was an invited speaker at the TED Global conference 2011, and his work on optical wireless communication was listed among the 50 best inventions in 2011 in the *Time* magazine.

Sándor Imre (Member, IEEE) was born in Budapest, Hungary, in 1969. He received the M.Sc. degree in electrical engineering, the dr.univ. degree in probability theory and mathematical statistics, and the Ph.D. degree in telecommunications from the Budapest University of Technology (BME), Budapest, Hungary, in 1993, 1996, and 1999, respectively, and the D.Sc. degree from the Hungarian Academy of Sciences, Budapest, Hungary, in 2007.

Currently he is Head of Telecommunications Department at BME. He is also Chairman of the Telecommunication Scientific Committee of the Hungarian Academy of Sciences. Since 2005, he has been the R&D Director of the Mobile Innovation Centre. His research interests include mobile and wireless systems, quantum computing, and communications. He has made wide-ranging contributions to different wireless access technologies, mobility protocols, security and privacy, reconfigurable systems, quantum-computing-based algorithms, and protocols.

Prof. Imre is on the Editorial Board of two journals: *Infocommunications Journal* and *Hungarian Telecommunications*.

Dominic O'Brien (Member, IEEE) received the M.A. and Ph.D. degrees from the Department of Engineering, University of Cambridge, Cambridge, U.K., in 1991 and 1993, respectively.

He is a Professor of Engineering Science at the University of Oxford, Oxford, U.K., and leads the optical wireless communications group. From 1993 to 1995, he was a NATO Fellow at the Optoelectronic Computing Systems Center, University of Colorado, Boulder. His current research is in the field of optical wireless systems. He is the author or coauthor of approximately 150 publications or patents in the area of optics and optoelectronics.

Markus Rupp (Senior Member, IEEE) received the Dipl.-Ing. degree from the University of Saarbrücken, Saarbrücken, Germany, in 1988 and the Dr.Ing. degree from Technische Universität Darmstadt, Darmstadt, Germany, in 1993, where he worked with E. Hänsler on designing new algorithms for acoustical and electrical echo compensation.

From November 1993 to July 1995, he held, with S. Mitra, a postdoctoral position with the University of California Santa Barbara, La Jolla, where he worked with A. H. Sayed on a robustness description of adaptive filters with impact on neural networks and active noise control. From October 1995 to August 2001, he was a Member of Technical Staff with the Wireless Technology Research Department, Bell Laboratories, Crawford Hill, NJ, where he worked on various topics related to adaptive equalization and rapid implementation for IS-136, 802.11, and the Universal Mobile Telecommunications System. Since October 2001, he has been a Full Professor of Digital Signal Processing in Mobile Communications with the Vienna University of Technology, Vienna, Austria, where he founded the Christian Doppler Laboratory for Design Methodology of Signal Processing Algorithms, at the Institute of Communications and Radio-Frequency Engineering, in 2002. He served as Dean from 2005 to 2007. He is the author or a coauthor of more than 350 papers and is the holder of 15 patents on adaptive filtering, wireless communications, and rapid prototyping, as well as automatic design methods.

Dr. Rupp is currently an Associate Editor for the *EURASIP Journal of Advances in Signal Processing* and the *EURASIP Journal on Embedded Systems*. He was an Associate Editor for the IEEE TRANSACTIONS ON SIGNAL PROCESSING from 2002 to 2005. He has been an Administrative Committee Member of EURASIP since 2004 and served as the President of EURASIP from 2009 to 2010.

Laszlo Gyongyosi (Member, IEEE) received the M.Sc. degree in computer science (with honors) from the Budapest University of Technology and Economics (BUTE), Budapest, Hungary, in 2008, where he is currently working toward the Ph.D. degree at the Department of Telecommunications.

His research interests are in quantum channel capacities, quantum computation and communication, quantum cryptography, and quantum information theory. Currently, he is completing a book on advanced quantum communications, and he teaches courses in quantum computation.

Mr. Gyongyosi received the 2009 Future Computing Best Paper Award on quantum information. In 2010, he was awarded the Best Paper Prize of University of Harvard, Cambridge, MA. In 2010, he obtained a Ph.D. Grant Award from University of Arizona, Tuscon. In 2011, he received the Ph.D. Candidate Scholarship at the BUTE; the Ph.D. Grant Award of Stanford University, Stanford, CA; the award of University of Southern California, Los Angeles; and the Ph.D. Grant Award of Quantum Information Processing 2012 (QIP2012), University of Montreal, Montreal, QC, Canada.